NATIONAL AERONAUTICS AND SPACE ADMINISTRATION

Technical Memorandum 33-314

High Energy Proton Testing of Mariner IV Components

Bruce E. Anspaugh

JET PROPULSION LABORATORY
CALIFORNIA INSTITUTE OF TECHNOLOGY
PASADENA, CALIFORNIA

January 1, 1967

NATIONAL AERONAUTICS AND SPACE ADMINISTRATION

Technical Memorandum 33-314

High Energy Proton Testing of Mariner IV Components

Bruce E. Anspaugh

Approved by:

W. S. Shipley

W. S. Shipley, Manager
Environmental Requirements Section

JET PROPULSION LABORATORY
CALIFORNIA INSTITUTE OF TECHNOLOGY
PASADENA, CALIFORNIA

January 1, 1967

TECHNICAL MEMORANDUM 33-314

Prepared Under Contract No. NAS 7-100
National Aeronautics & Space Administration

Preface

The following personnel contributed sections of this report for the subjects noted, in addition to performing the measurements reported:

C. Carl	Data Encoder
L. H. Swanson	Pin Puller Squibs
T. Groudle	Liquid Propellant Actuator Squibs
W. L. Long	Batteries
P. Berman	Solar Cells
D. D. Lord	Central Computer and Sequencer
C. J. Marlett	Microcircuits
D. Bergens	Semiconductor Devices
J. T. Kinsey	Data Automation Subsystem

Others who contributed substantially to this study are A. M. Koehler and the entire Harvard cyclotron staff; M. M. Nicholson, of Atomics International; and G. L. Juvinall, L. F. Schmidt, and T. K. Johnston, of the Jet Propulsion Laboratory.

Contents

Contents (contd)

Tables

Contents (contd)

Tables (contd)

Figures

Abstract

The following *Mariner IV* components were irradiated with 20 to 137 Mev protons from the Harvard synchrocyclotron: (1) Canopus tracker, (2) data encoder, (3) squibs, (4) batteries, (5) solar cells, (6) central computer and sequencer circuitry (CC&S), (7) sun sensor, (8) semiconductor devices and integrated circuits. Flux rates used varied between 5×10^4 and 3×10^7 protons/cm^2 sec. All tested units were irradiated to an integrated flux of at least 2×10^{10} protons/cm^2. All components, except the solar cells and Canopus tracker, operated normally during irradiation. The power output of the solar cells permanently dropped to approx. 85% of the pre-irradiation value but was less than the predicted power loss. The tracker lost roll control at flux rates greater than 6×10^5 protons/cm^2 sec for energies greater than 40 Mev, but recovered tracking ability immediately when the beam cut off, even after an integrated flux of 2.4×10^{10} protons/cm^2. Consequently, a high energy, high intensity solar flare could degrade tracker operation to a marginal region, but the system will recover after the flare. The tracker sensitivity was found to be due to an induced radioactivity in the image dissector tube.

High Energy Proton Testing of *Mariner IV* Components

I. Introduction

Mariner 67 and 69 will be launched in a time period during which an encounter with high energy solar flare protons is nearly certain. This is due to the expectation that the next solar cycle maximum will occur in 1969, and the observation that solar flare events producing high energy protons are more likely to occur one or two years before and after the maxima. Based on previous measurements and the best extrapolation we can make into the future, flux rates as high as 2.7×10^5 protons/cm^2 sec and yearly integrated fluxes of 2×10^{10} protons/cm^2 ($E > 20$ Mev) may be encountered (Ref. 1).

Consequently, we have examined the behavior of several *Mariner IV* components to assess their operational performance in this radiation environment. The items were singled out for testing on the basis of their demonstrated susceptibility to electron radiation (Ref. 2)—those which would, in our opinion, probably be sensitive, or for which we have no information concerning their behavior during proton radiation.

The synchrocyclotron at Harvard University was chosen as the proton source because it could produce the energies and flux rates needed for simulation of both radiation fields, namely, 20 to 137 Mev and 10^4 to 10^7 protons/cm^2 sec over the subsystem surfaces.

II. General Test Setup and Calibration

A. Facility and Arrangement

The test setup used at the Harvard synchrocyclotron site is diagrammed in Fig. 1. The machine produces 160 Mev protons in a beam which is focussed on lead scatterer SC. The protons undergo multiple scattering collisions in SC and emerge with reduced energy, but with sufficient angular divergence to produce a circular cross section of 18-in. diam at the test plane. The ion chamber S is used to monitor beam intensity. Polyethylene absorbers may be placed in front of the test plane to reduce beam energy. Without the absorbers, beam energy at the test plane is 137 Mev.

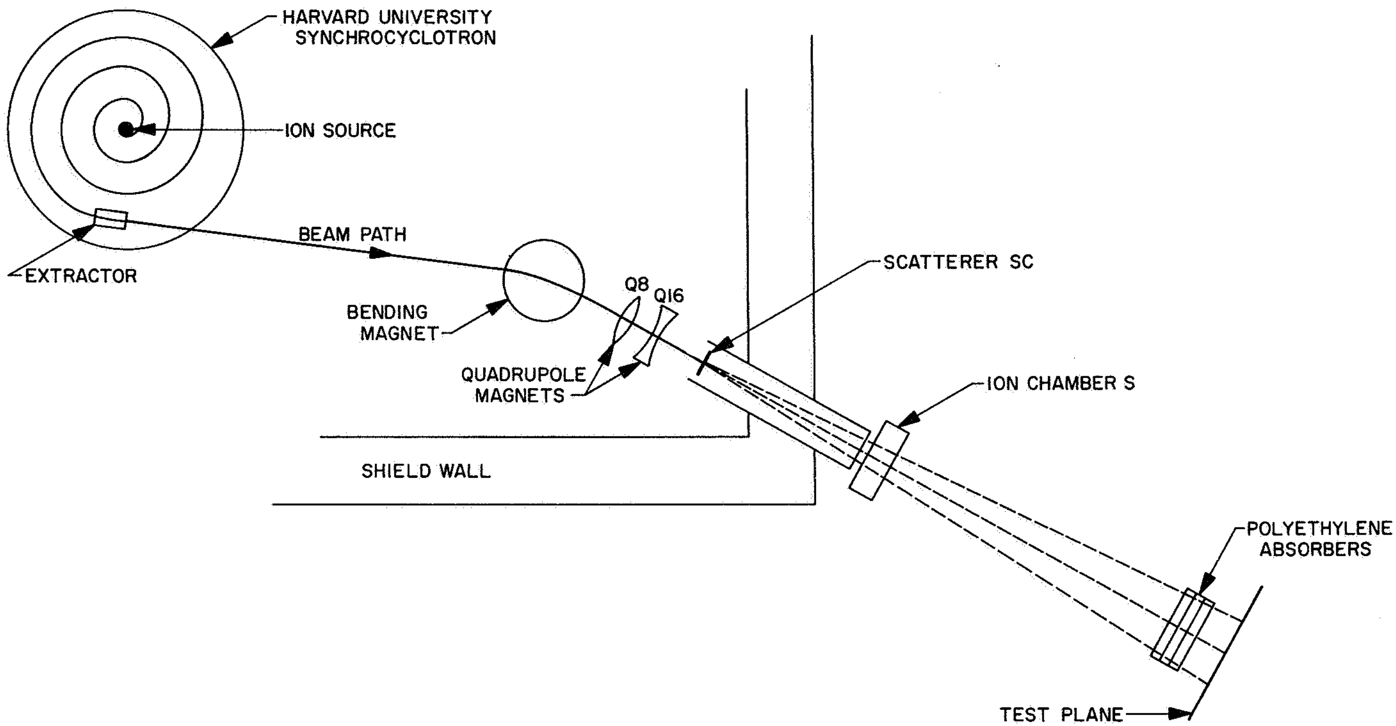

Fig. 1. Diagram of Harvard synchrocyclotron facility

The subsystems were connected by 50-ft cables to the OSE located in the accelerator control room.

B. Calibration and Alignment

Having focussed the beam on the scatterer, the beam intensity profile was mapped at the test plane by means of a small defined volume ionization chamber (DVIC). Results of the horizontal and vertical mapping traverses are shown in Figs. 2 and 3.

Absolute beam flux calibration was achieved by placing a Faraday cup and lead collimator at the beam center in the test plane. It was found that the flux at the beam center in the test plane could accurately and repeatably

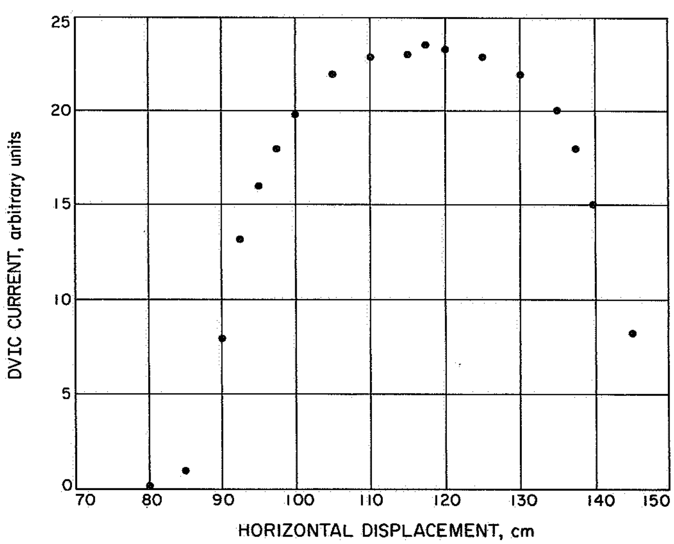

Fig. 2. Beam mapping in horizontal plane

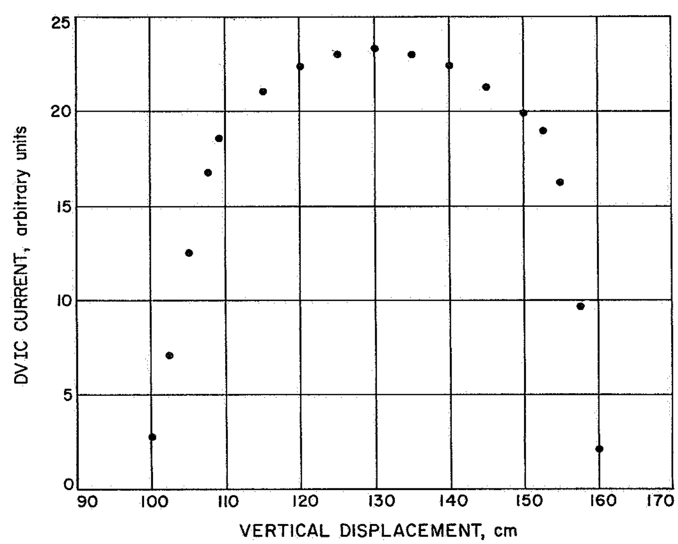

Fig. 3. Beam mapping in vertical plane

be related to the current collected in ionization chamber S. This calibration procedure allowed subsequent bombardment of objects lying in the test plane without the necessity of also mounting a Faraday cup nearby.

III. General Test Procedure

The test item, centered in the test plane, was first irradiated at 137 Mev with a low flux rate for a time sufficient to assess performance while operating in the beam. Fluxes were gradually increased to search for a possible failure threshold flux, with frequent beam interruptions to search for permanent damage effects, and for a thorough system check out. If no malfunctions occurred with maximum available flux from the cyclotron, the item was irradiated to 2×10^{10} protons/cm^2. At this point the beam energy was reduced and the above procedure repeated. If several identical test items were available, a new item was used each time the beam energy was changed. A variation on the above procedure occurred when a test item was not instrumented for beam-on monitoring. In this case the item was bombarded only with a high flux rate until an integrated flux of 2×10^{10} protons/cm^2 was reached. A further variation was carried out in the final stages of the test program wherein we bombarded some of the semiconductor devices at medium to high flux rates, omitting the low rate testing. This was done in the interest of saving time only after having observed the high tolerance of previously irradiated devices of similar type.

IV. Data Encoder

A. Test Setup

The *Mariner C* data encoder used for the test was the prototype, S/N 1, which had approximately 9,950 hours running time at the conclusion of the test. Anticipating that some permanent damage might result from proton radiation, the most sensitive parameters that could be reasonably monitored were measured prior to the test. These were the low-level amplifier open-loop gain, the power supply voltages (under specific load), the analog-to-digital converter indecision points, and the constant current source output.

The encoder was placed in the proton beam path, with connections made via cabling running through conduits under the shield wall to the OSE in the control area. Connections consisted primarily of those available in a launch (long-line) configuration; namely, synchronization terms and mixed signal to operate the OSE decommutator. The launch umbilical amplifier was used for drive and isolation. Representative samples of each channel type (nine 1.5-v channels, eighteen 3-v channels, seven 100-mv channels, four pressure channels, and eleven temperature channels) were exercised from a battery source located at the encoder (to avoid long cables). As a back up, in case this minimal cabling was prohibitive, a ground telemetry console with demodulator and decommutator was used. Connections were made between the two OSE's to implement bit-error rate monitoring (BERM). Additional capability existed to make a low-level amplifier open-loop gain check from the OSE during irradiation.

B. Test Procedure

The data encoder with circuit board number 4 taped to its front face (descriptions of circuit board tests are given in Section XI) was positioned with respect to the beam center as shown in Fig. 4. The combination was then irradiated with 137 Mev protons for about 7 min at a low flux (2.2×10^4 protons/cm^2 sec) while data encoder operation was monitored. Since the operation was

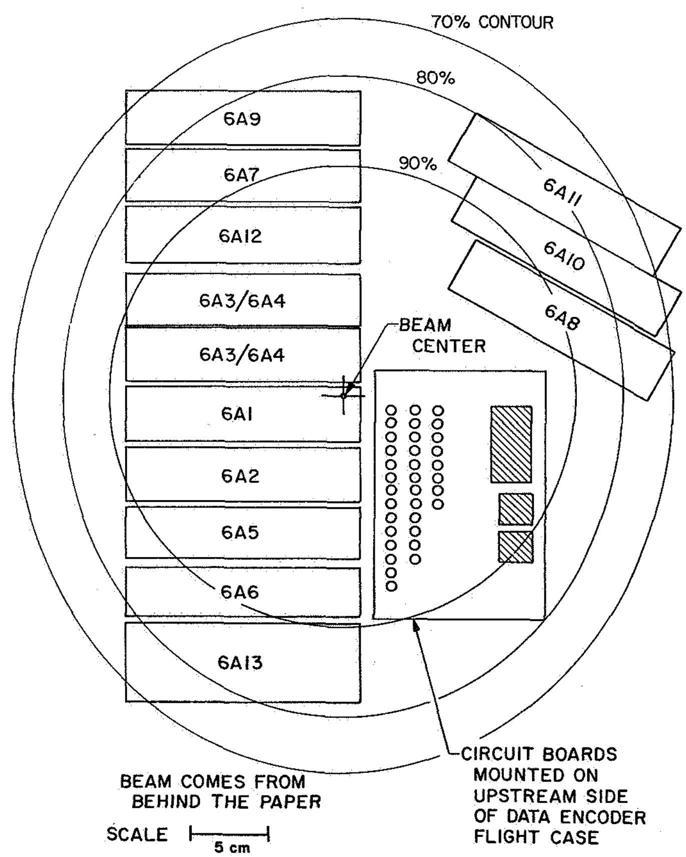

Fig. 4. Beam isoflux contours superimposed on data encoder

normal, the flux was increased and data encoder functions again checked. The flux increases continued until the high current limit of the cyclotron was reached. Since no flux rate dependent failures had occurred, we continued irradiation at the highest flux available (8×10^6 to 1.0×10^7 protons/cm^2 sec) to check for permanent damage effects. When an integrated flux of 1.6×10^{10} protons/cm^2 was reached, the proton beam was interrupted and circuit board 4 removed to a radiation-free area. The data encoder irradiation then continued until an integrated flux of 4.4×10^{10} protons/cm^2 at 137 Mev was reached. The cyclotron was then shut off to allow an extensive checkout of the data encoder functions.

The above procedure was repeated essentially as described for a 99 Mev bombardment. Here circuit board 3 received 1.1×10^{10} protons/cm^2 integrated flux and the data encoder 4.1×10^{10} protons/cm^2. The beam energy was decreased to 99 Mev by inserting 5.4 grams/cm^2 of polyethylene absorber into the beam path directly in front of the data encoder.

Irradiation at 59 Mev and 33 Mev proceeded in analogous fashion. The 59 Mev run required 9.5 grams/cm^2 of polyethylene absorber and 11.2 grams/cm^2 was used for the 33 Mev run. In the 59 Mev run circuit board 2 received 1.1×10^{10} protons/cm^2 integrated flux and the data encoder 4.1×10^{10} protons/cm^2. In the 33 Mev run circuit board 1 received 1.2×10^{10} protons/cm^2 and the data encoder 4.3×10^{10} protons/cm^2. The total integrated flux (all energies) received by the data encoder was 1.7×10^{11} protons/cm^2, which amounts to a *surface* dose of 2.2×10^4 rads (aluminum).

At the completion of each group of tests having the same energy level, a complete subsystem test was performed, including those measurements mentioned above.

C. Test Results

The resultant effects on the data encoder of the composite radiation were negligible; if an equivalent radiation were encountered in flight *it would be difficult to determine whether the changes were due to radiation or to the expected variations due to aging and normal sensor value shifts.* There were no deck resets or skips, event counter changes, out-of-lock indications; nor was any other transitory behavior observed. The BERM indicated only 3 bit-errors during the tests. Only three channels of the 49 excited changed in value, and each of those by only one data number.

Table 1. Radiation effects on the ADC indecision points[a]

Analog-to-digital converter A indecision points (off during radiation)					
BCD transitions	After 4.4×10^{10} p/cm^2 at 137 Mev[a], mv	After 4.1×10^{10} p/cm^2 at 99 Mev, mv	After 4.1×10^{10} p/cm^2 at 60 Mev, mv	After 4.3×10^{10} p/cm^2 at 30 Mev, mv	Total net change, mv
0–1	5.2–6.1	4.3–5.0	3.7–4.6	2.9–3.2	−2.6
1–2	29.5–29.9	28.2–28.6	27.3–27.8	26.7–27.2	−2.8
3–4	75.7–76.2	74.9–75.4	74.1–74.4	73.2–73.6	−2.5
7–8	170.0–170.8	168.6–169.2	168.1–168.3	167.2–167.8	−2.9
15–16	357.2–357.6	356.3–356.8	355.5–356.0	354.5–355.0	−2.7
31–32	730.6–731.3	729.8–730.3	728.7–729.5	728.2–728.5	−2.6
63–64	1477.2–1478.6	1476.7–1477.3	1475.6–1476.2	1474.7–1475.4	−2.9
Analog-to-digital converter B indecision points (on during radiation)					
BCD transitions	After 137 Mev run[a], mv	After 99 Mev run, mv	After 60 Mev run, mv	After 30 Mev run, mv	Total net change, mv
0–1	10.4–10.8	9.5–10.0	8.9–9.4	8.8–9.4	−1.5
1–2	33.5–33.9	32.8–33.5	32.6–33.0	32.2–36.6	−1.2
3–4	81.1–81.5	79.9–80.3	79.9–80.2	79.6–80.1	−1.5
7–8	174.5–175.3	174.0–174.4	173.4–173.9	173.5–173.9	−1.5
15–16	362.0–362.6	360.8–361.3	361.0–361.6	360.7–361.1	−1.4
31–32	736.0–736.6	734.5–735.5	735.2–735.4	734.8–735.3	−1.3
63–64	1480.8–1481.6	1480.0–1480.9	1479.6–1480.4	1479.5–1480.4	−1.2

[a]Data prior to 137 Mev run (i.e., initial point) was not used because of poor test set up.

Table 2. Averaged data encoder parameter data

Parameter	Before irradiation	After 137 Mev (4.4×10^{10} p/cm^2)	After 99 Mev (4.1×10^{10} p/cm^2)	After 60 Mev (4.1×10^{10} p/cm^2)	After 30 Mev (4.3×10^{10} p/cm^2)
+6v	6.316	6.315	6.315	6.314	6.317
−6v	−6.224	−6.235	−6.235	−6.233	−6.233
+20v	19.979	19.964	19.961	19.960	19.959
−20v	−19.938	−19.929	−19.924	−19.922	−19.921
+3v	2.9973	2.9956	2.9953	2.9951	2.9950
Low-level amp gain	~1150	~1130	~1112	~1106	~1100
Constant current source output	0.995 ma	0.995 ma	0.995 ma	0.995 ma	0.995 ma

Tables 1 and 2 depict the data results. As preface comments, in Table 1, it should be noted that the pretest data, those data before the 137 Mev run, are missing. These data were taken using a higher input impedance source to the ADC than on subsequent tests. The increased noise of the source produced a wider indecision zone (several mv) which masks the change during the 137 Mev test. In Table 2, it should be noted that these are average data values; the raw data had some scatter and hence averaging was necessary. The scatter was due to imperfect repeatability of OSE-encoder test setup and temp. environment: trying to confirm mv changes after irradiation was difficult. Hence, the data in Table 2 should be viewed more to observe trends (small as they are) rather than absolute deltas.

The data on the internal measurements explain why system level detection of change would be difficult. Tables 1 and 2 indicate a uniform degradation in performance, the rate being more pronounced at the initial tests. A few points of interest: The ±6v showed much less variation than the ±20v, which are regulated supplies. The +3v (regulated from the +20v) showed the same percentage variation as the other regulated supplies. The low-level amp gain change cannot be accounted for by these power supply changes; it is an independent effect. The gain change is equivalent to 0.1% change closed loop, or 3 mv full scale. Note that ADC-A had about 2.7 mv change in indecision points, while ADC-B had half that amount of change. This is interesting since ADC-A was off during the tests.

One hesitates to speculate on the cause of these fine-structure changes; the component interactions are very complex. Transistor beta decreases probably account for most of the noted effects.

A bit interval is about 23 mv. These changes amount to about 1/10 to 2/10 of a bit interval. Probabilistically, only a small percentage of the channels would show any change at all. This is borne out in the data: 3 of 49 changed. It also explains why system-level detection of changes due to irradiation would be difficult. In conclusion, there is no evidence that a flight data encoder would experience significant change in performance due to this type of proton radiation.

V. Squibs

A. Test Setup

1. Pin puller types

Squibs were exposed in pin pullers, as well as with the metal end-closure of the squib removed so as to expose the explosive material directly to the radiation beam to obtain a worst case situation. Four squibs and one pin puller were exposed at each of the two energy levels used, 137 and 60 Mev.

Due to the limited quantity of flight squibs on hand, the test program was augmented with available squibs which differ from the flight type in the method of sealing the explosive in the squib body. As the end closures were removed for this experiment, the data obtained are considered valid.

The squibs were bombarded at a high flux rate only, roughly 3.9×10^7 protons/cm^2 sec., to an integrated flux of 2.1×10^{10} protons/cm^2.

After return to JPL the units were tested electrically, and then fired for time pressure and functioning data, as given in Tables 3, 4, and 5.

Electrical tests after exposure (dielectric and bridgewire resistance) were normal.

Table 3. Pin puller functioning data

S/N	Energy, Mev	Flux, protons/cm^2	Firing time, ms	Total pin puller function time, ms	Test temp, °F	Remarks
208	60	2.1×10^{10}	0.64	1.159	−320	Squib exposed to radiation while installed in pin pullers
246	137	2.1×10^{10}	0.46	1.101	−320	

One live squib and one inert squib utilized to function pin puller.

Squib fired with 795 μf capacitor charged to 25 v. 1.3 Ω series resistance in squib firing circuit.

50 lb side load on piston pin.

Table 4. Functioning data for unirradiated pin pullers

Date of test	Firing time, ms	Total pin puller function time, ms	Test temp, °F
May 66	1.28	1.685	−320
May 64	0.37	0.846	−75
May 64	0.31	0.789	−75
May 64	0.51	1.070	+75
May 64	0.48	0.985	+75

The firing time and function time of the May 66 test might appear long. However, it is normal for the level of firing currently used. This squib was fired at 4 amp (const. current).

The May 64 firings used a 795 μf capacitor charged to 25 v.

Table 5. Squib firing data

S/N	Energy, Mev	Flux, protons/cm^2	Firing[a] time, ms	Peak pressure, psi	Time to peak, ms	Test temp, °F	Remarks
479	—	—	7.6	5800	0.2	+75	Control[b]
313	60	2.1×10^{10}	7.4	5800	0.2	+75	Direct[c]
407	137	2.1×10^{10}	6.6	5700	0.2	+75	Direct
195	—	—	6.5	4600	0.1	+75	Control
484	—	—	6.4	6200	0.1	+203	Control
496	60	2.1×10^{10}	7.1	3900	0.4	+203	Direct
241	137	2.1×10^{10}	6.9	5100	0.2	+203	Direct
462	—	—	8.8	4800[d]	0.2	−320	Control
064	60	2.1×10^{10}	10.8	5500[d]	0.1	−320	Direct
366	137	2.1×10^{10}	12.4	5400[d]	0.2	−320	Direct
445	60	2.1×10^{10}	13.3	3900[d]	1.5	−320	Direct
540	137	2.1×10^{10}	22.8	—	—	−320	Direct

[a]Above firings at 1.5 amp (const. current).

[b]Control: These squibs were not irradiated.

[c]Direct: Squibs have end closures removed and explosive material facing source of radiation.

[d]Pressures recorded at cold temp. are considered indicated pressures only (due to inability to calibrate transducer at this temp.).

Squib firing data obtained from this test are comparable to previous test results for this particular squib.

Pin puller functioning data are also comparable to previous test data.

From the data obtained, it is felt that proton radiation, of the levels utilized for this test, has no significant degrading effect on the pin puller pyrotechnics.

2. Liquid propellant valve actuator types

These squibs were bombarded concurrently with the pin puller squibs in the same fixture. They also received protons at the rate of 3.9×10^7 protons/cm^2 sec. and an integrated flux of 2.1×10^{10} protons/cm^2. Bare squib S/N 24817 and squib S/N 24805 mounted in a valve fixture were irradiated at 137 Mev. Bare squib S/N 24811 and squibs S/N 24792 and S/N 24788 in valves were irradiated at 60 Mev.

B. Test Results

Two squibs were subjected to squib tester operation and three squibs to the closed bomb (fixed volume) operation. After firing, all squibs were subjected to internal helium pressurization leak tests at 10 and 1,000 psig. The post radiation test calibration was accidentally omitted on two of the squibs in the closed bomb tests. Test results are shown in Table 6. Based on the results of these tests, there appears to be no degradation of the propulsion system pyrotechnics.

VI. Batteries

A. Test Setup

1. Ag-Zn, Ag-Cd, and Ni-Cd cells

The following set of cells was irradiated at 137 Mev; an identical set was irradiated at 60 Mev. Total flux for

Table 6. Value actuator squib test results

Sterilized squibs (JPL p/n J4700697) subjected to proton radiation

Squib S/N	Pretest calibration				Post-test calibration				Max. firing, v	Closed bomb firings					
	Resistance		Dielectric		Resistance		Dielectric			Max. press, psi	Max. accel, g	Time, msec			
	ab	cd	str.	res.	ab	cd	str.	res.				To fire	To first press.	Press. rise	To max. press.
24811	1.11	1.08	passed	passed	[a]	[a]	[a]	[a]	7.8	19,000	5,400	0.62	0.70	1.40	2.0
24817	1.10	1.10	↓	↓	[a]	[a]	[a]	[a]	7.8	32,000	6,800	0.61	[b]	0.80	1.4
24792	1.11	1.10	↓	↓	1.10	1.09	passed	passed	7.9	27,000	10,000	0.58	0.65	1.35	2.0
24805	1.07	1.07	↓	↓	1.04	1.03	↓	↓	8.0	—	—	—	—	—	—
24788	1.11	1.04	↓	↓	1.07	1.06	↓	↓	8.0	—	—	—	—	—	—
Acceptable values	1.00 to 1.30	1.00 to 1.30	passed	passed	1.00 to 1.30	1.00 to 1.30	passed	passed	3.0 to 10.0	10,000 to 46,000	3,000 to 15,000	0.55 to 1.15	0.62 to 1.02	0.34 to 1.44	1.06 to 2.20

Squib S/N	Squib tester firings								Leakage, std-cm^3/sec		Irradiation	
	Max. press, psi	Max. force, lb	Max. piston travel, in.	Total energy, ft-lb	Time, msec				At 10 psi helium	At 1,000 psi helium	Energy, Mev	Flux, protons/cm^2
					To fire	To press.	Press. rise	To max. press.				
24811	—	—	—	—	—	—	—	—	4.3×10^{-7}	7.5×10^{-6}	60	2.1×10^{10}
24817	—	—	—	—	—	—	—	—	3.3×10^{-7}	4.9×10^{-6}	137	2.1×10^{10}
24792	—	—	—	—	—	—	—	—	9.5×10^{-7}	7.4×10^{-6}	60	2.1×10^{10}
24805	11,000	2,200	0.22	273	0.57	[b]	0.16	0.73	2.9×10^{-7}	6.2×10^{-6}	137	2.1×10^{10}
24788	10,000	2,200	0.28	532	0.57	0.65	0.10	0.75	4.2×10^{-7}	4.0×10^{-6}	60	2.1×10^{10}
Acceptable values	7,000 to 11,200	2,100 to 2,300	0.22 to 0.54	258 to 900	0.53 to 0.67	0.63 to 0.81	0.10 to 1.10	0.73 to 1.80	1.0×10^{-6} max	1.0×10^{-5} max		

[a]Test omitted.

[b]Time to first pressure coincidental with "to fire" time.

each set was about 2×10^{10} protons/cm²: One 3-cell monoblock, Ag-Zn, Electric Storage Battery model 263, 50 amp-hr capacity (*Mariner* C type); two Ag-Cd, Electric Storage Battery model 293, 15 amp-hr capacity cells; three Ni-Cd, GE no. 41B004AA05, 2 amp-hr capacity-size cells.

The cells were placed near the center of the 18-in. proton beam. The cylindrical Ni-Cd cell had the curved side facing the beam. The rectangular Ag-Cd and Ag-Zn cells were placed with edges facing the beam so that no plate was shaded by another. An identical set of cells was used as a control; these cells received the same treatment as the others, except they were not irradiated. During irradiation the open circuit cell voltages were monitored.

2. *Ni-Cd and Ag-Cd research cells*

It was considered valuable to test rather simple research cells in addition to the batteries because of the large number of variables present in a complete battery. In addition, the experimental cells were designed to be as similar as possible to those currently used in the study of the effects of gamma radiation on battery electrodes by Atomics International. This feature will enable the results of the two programs to be correlated, enhancing the value of each.

The experimental cells were composed of inner polystyrene cell liners containing the electrodes and electrolyte, and an outer gas tight glass container. All cells were run at a 90% charge level. The cell liners contained three compartments separated by fritted quartz discs. The electrode under study (silver or nickel) was placed in the center compartment and the two non-limiting electrodes occupied the two outer compartments. The design of the cell liner is illustrated in Fig. 5.

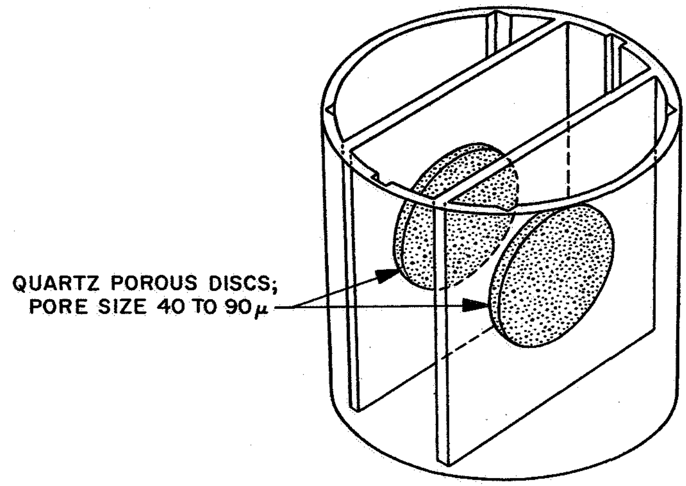

Fig. 5. Polystyrene cell liner

The electrolyte in all cells was 40% potassium hydroxide. The cell liners containing the electrodes and electrolyte were placed in glass containers fabricated with pyrex O-ring type joints. The completed cells were then purged and filled with nitrogen. Each was equipped with a pressure gauge and break seal. During beam-on testing, the pressure gauges were observed by means of closed circuit television.

B. Test Results

1. *Ag-Zn, Ag-Cd and Ni-Cd cells*

No electrical or visual changes could be observed during or after irradiation (Table 7). Cell voltages remained constant within voltmeter resolution. The cells became slightly radioactive; maximum observed radioactivity was less than 20 milliroentgens/hr at cell surface immediately after the 137 Mev irradiation. Within 6 hr the radioactivity had decayed to less than 0.5 milliroentgens/hr.

After the cells were returned to JPL, capacity checks indicated no degradation had occurred.

Therefore, we conclude that solar flares of about 10^{10} protons/cm² will have no apparent effect on spacecraft batteries.

2. *Ni-Cd and Ag-Cd research cells*

Atomics International Division of North American Aviation, Inc., was responsible for the analysis of the cells after irradiation. Capacity measurements on the silver electrodes were reproducible to ±1%.

No capacity changes occurred in the silver limited cells due to radiation although a 10% increase was observed as an aging effect. Gas evolution and pressure change were negligible in the silver cadmium cells, and quantities of solid material lost appear to be the same as in the control cells (Ref. 3).

The only nickel electrodes available at the time of this program proved to be unstable when operated in a flooded condition. For this reason, the capacity data on the nickel-cadmium cells were unsatisfactory, and material losses were erratic. Little or no gas was evolved as a result of proton irradiation.

Table 7. Post-irradiation measurements made on irradiated and control cells

Type	Manufacturer	Model	Serial no.	Open circuit voltage, v	Capacity, amp-hr	
					Discharge	Charge
2.0×10^{10} protons/cm² at 137 Mev						
Ag-Zn	ESB	263	14	1.86–1.87	43	52
Ag-Cd	ESB	293	22	1.42	15	17
Nn-Cd	GE	41B004AA05	8	1.34	1.1	About 2
2.0×10^{10} protons/cm² at 60 Mev						
Ag-Zn	ESB	263	12	1.87	43	52
Ag-Cd	ESB	293	20	1.42	15	17
Ni-Cd	GE	41B004AA05	5	1.34	1.1	About 2
Control cells						
Ag-Zn	ESB	263	17	1.87	43	52
Ag-Cd	ESB	293	21	1.42	15	17
Ni-Cd	GE	41B004AA05	6	1.34	1.1	About 2

C. Discussion

On the basis of the data obtained thus far, it may be concluded that proton radiation in the dose range used in these experiments has no apparent effect on the battery electrodes. However, a much larger dose may produce an effect, probably loss of solid material from the electrodes. In any event, none of the data indicates that the expected solar flare activity during 1967-69 will prove to be a problem insofar as the batteries are concerned.

VII. Solar Cells

A. Description of Test Items

The following silicon solar cells in various configurations, and *Mariner* Venus 67 cell submodules were considered in this experiment in order to isolate the regions of significant radiation damage to the submodules and to provide comparisons between the radiation effects and various cell designs: (1) P/N 1 Ω-cm (*Mariner C* type), (2) N/P 1 Ω-cm and 10 Ω-cm (radiation resistant type). The cells were irradiated to an integrated flux of 2.1×10^{10} protons/cm² at energies of 137, 100, and 36 Mev. A group of cells composed of the items listed in Table 8 was irradiated at each of the three energy levels.

Items 1–4 and 8 and 9 are directly applicable to the *Mariner* Venus 67 program. The other items were included as a basis of comparison. In addition to the above items, at each energy level 2 P/N filtered cells and 1 N/P 8-mil-thick filtered cell was monitored under illumination during the proton irradiation to study transient effects. The test specimens were so selected that any observed electrical degradation could then be traced back to effects in the coverslip, effects in the coverslip-adhesive combination and effects in the cell itself.

Table 8. Solar cells irradiated

Item	Quantity	Description
1	2	*Mariner* Venus 67 7-cell submodules.[a]
2	5	P/N[a] (*Mariner* Venus 67 type) filtered cells (6-mil coverslip) identical to cells of item 1.
3	5	P/N[a] cells similar to item 2 but without filters (bare).
4	5	P/N[a] cells similar to item 3 but with rtv coverslip adhesive applied to active face.
5	5	N/P cells, 1Ω-cm base resistivity, 6-mil coverglass
6	5	N/P cells, 10Ω-cm base resistivity, 6-mil coverglass
7	4	N/P cells, 10Ω-cm base resistivity, 8-mils thick, 2 × 2 cm² area, 6 mil coverslip
8	5	Coverslips
9	2	Coverslip, adhesive, coverslip, sandwiches.

[a]All P/N cells had initial resistivity of 1Ω-cm.

B. Test Setup

The cells were mounted on an aluminum 1/16×15×15 in. plate. Three such plates, one at each energy level, were utilized. Provisions were made on the plates for illuminating the three transient monitoring cells described above and observing their short circuit current output with a Simpson meter model 260 located in the control room.

C. Experimental

Transient effects. The transient monitoring cells were illuminated with an ultraviolet sunlamp during the first part of the 137 Mev irradiation. Since no transient effects were seen, the above light source was exchanged for a 150-w tungsten bulb. The longer wavelength light from the tungsten source penetrates farther into the cell, with the result that the short circuit current should now be a more sensitive measure of radiation damage. The tungsten light source was used for the remainder of the 137 Mev irradiation and for the 100 Mev and 36 Mev irradiations as well. Even with this light source no transient effects were observed. Furthermore, the ratio of the short circuit current to the initial short circuit current showed the expected linear relationship to the logarithm of the flux which is characteristic of permanent degradation.

Permanent effects. Pre-irradiation and post-irradiation current-voltage curves were obtained for each cell and for each submodule. Curves were also obtained for two control submodules and several groups of control cells which were not irradiated, under illumination by an OCLI solar simulator calibrated to correspond to air mass 0 solar spectrum and under a tungsten simulator having a color temperature of 2,800°K. A control solar cell was used as a detector cell for the coverslips and coverslip-adhesive sandwiches. Each of the filters and sandwiches was placed on top of the detector cell and the current-voltage curve of the cell was obtained.

D. Test Results

As mentioned previously, no transient effects were observed, even at flux rates as high as 10^7 protons/cm^2 (which are higher than the expected flux rates which would be experienced due to solar flares). This was the case independent of whether a high blue (mercury vapor lamp) or a high red (tungsten lamp) illumination source was used.

The illumination from the OCLI solar simulator is uniform to $\pm 2\%$ over an area of about 2 cm $\times$ 6 cm. The area of a 7 cell submodule is about 2 cm $\times$ 7 cm. When the post-irradiation measurements were made it was found that the control modules were about 4% lower in short circuit current than was measured during the pre-irradiation sequence; thus these measurements are considered to be somewhat unreliable. A measurement accuracy, that is control cell reproducibility, of better than 2% is desired for meaningful results. The reason for utilizing the tungsten light source now becomes apparent. Not only does this provide a second set of independent measurements (the two illumination systems having been set up by means of different balloon flight standard cells), but the tungsten light source is extremely stable and has a large, uniform area of illumination. Unfortunately, the spectral content of the tungsten light is considerably different from natural sunlight, so that the results obtained under tungsten illumination must be used with discretion. It was expected a priori that the electrical degradation experienced by the P/N cells with the 6-mil coverglasses (Table 8, item 2) would be identical to that experienced by the submodules. By comparing the pre- and post-radiation data obtained from these cells and the submodules under tungsten light, which should magnify any differences, this expectation was found to be valid. A summary of the data is presented in Table 9.

Table 9. P/P_0 ratio for P/N cells and P/N submodules as measured in tungsten simulator

Sample	Proton energy level, Mev	P/P_0 range
P/N with 6-mil coverslip (5 cells at each level) (P_0 = 14 mw/cm^2)	36	0.73–0.80
	100	0.74–0.84
	137	0.82–0.88
	0	1.00–1.00
7 cell submodules (2 modules at each level)	36	0.76–0.78
	100	0.83–0.83
	137	0.84–0.85
	0	1.00–1.00

Thus, it can be safely concluded that there is no significant difference in radiation damage between submodules and the individual cells from which the modules are made for the proton energy levels considered in this experiment. Hence, the results as obtained in the solar simulator for the P/N cells with 6-mil-thick coverslips are applicable to sub-modules as well. The reproducibility of the control cell measurements in the simulator was quite good (the control cell readings were reproduced to better than 2%) so that it may be concluded that the problem encountered in measuring the sub-modules in the simulator was due to the large area of the module, which was somewhat beyond the capabilities of this particular simulator.

It was found that there was no significant damage done by the protons to the coverslips and the coverslip-adhesive sandwiches since the pre-irradiation and post-irradiation measurements were identical within the $\pm 2\%$ measurement error.

A summary of the *preliminary results* obtained in the OCLI solar simulator is presented in Table 10.

Table 10. Preliminary measurements of solar cell degradation after 2×10^{10} protons/cm² (OCLI simulator)

(5 Cells of each type at each energy level)				
Cell Type	Proton energy, Mev[c]	I_{sc}/I_{sc_0} range	V_{oc}/V_{oc_0} range	P/P_0 range
P/N[a] (6-mil coverslip)	36	0.85–0.87	0.94–0.97	0.81–0.84
	100	0.86–0.91	0.96–0.97	0.83–0.88
	137	0.90–0.94	0.97	0.87–0.91
	0	1.00	0.98–1.00	0.98–1.00
P/N[a] (no coverslip)	36	0.84–0.90	0.94–0.96	0.81–0.86
	100	0.89–0.92	0.95–0.97	0.85–0.90
	137	0.90–0.92	0.96–0.97	0.87–0.89
	0	1.00	0.99	0.98–0.99
P/N[a] adhesive only	36	0.87–0.91	0.94–0.96	0.82–0.85
	100	0.87–0.92	0.96–0.97	0.85–0.88
	137	0.91–0.93	0.97–0.98	0.88–0.90
N/P[b] 1Ω-cm base (6-mil coverslip)	36	0.95–0.96	0.97–0.99	0.92–0.94
	100	0.96–0.97	0.98–1.00	0.95–0.97
	137	0.97–0.99	0.98–0.99	0.95–0.98

[a] $P_0 = 14$ mw, $I_{sc_0} = 33$ ma, $V_{oc_0} = .58$v.
[b] $P_0 = 14$ mw, $I_{sc_0} = 34$ ma, $V_{oc_0} = .55$v.
[c] Flux $= 2.1 \times 10^{10}$ protons/cm²

It can be seen from Table 10 that the P/N cells with coverslips, without coverslips, and with adhesive only, exhibit similar electrical degradation as a result of the proton irradiation at any given energy level, and if one wished, the results of the three types of P/N cells could be pooled to give a sample size of 15 units at each energy level. This bears out the results obtained from the coverslip and cover-adhesive sandwiches experiment; that is, there is no significant damage, at least as far as the solar cell electrical characteristics are concerned, occurring in either the coverslip or the adhesive used to bond the coverslips to the active cell face. The electrical degradation is a result of damage to the cell itself for these energy ranges and flux densities. Furthermore, the coverslip provides no significant attenuation of protons in these energy ranges.

E. Comparison with Theory

A method for predicting the power degradation as a function of proton energy and flux (in terms of the ratio of power after exposure to initial power) which would be experienced by N/P and P/N cells fabricated from 1 Ω-cm resistivity material has been developed. The method makes use of the damage coefficient of the respective cell types as a function of proton energy to obtain the equivalent 1 Mev electron flux for each cell type as a function of proton energy. Experimental curves which relate the P/P_0 ratio to a unidirectional flux of 1 Mev electrons can then be utilized to predict the power degradation for a flux of protons of a given energy. The equivalent 1 Mev electron fluxes as a function of proton energy are actually appropriate to an omnidirectional flux of protons with infinite back shielding of the cell; thus, only ½ the total flux is actually incident upon the cell. (This is normally the case for calculations involving solar protons, and thus the curves can be used directly.) In this case, however, since we have a unidirectional flux of protons, the total equivalent 1 Mev electron flux obtained by multiplying the proton flux by the equivalent electron flux (for the proton energy of interest), must be multiplied by a factor of 2.

Table 10 shows the preliminary results for the three types of P/N cells investigated, that is, filtered, unfiltered and with filter adhesive only, and for the N/P 1 Ω-cm base cells with filters.

Figure 6 shows the results from Table 10 for the P/N and N/P cells with 6-mil-thick coverslips. The P/P_0 range for these two cell types is plotted as a function of the equivalent 1 Mev electron unidirectional flux density. Also shown in this figure are the predicted degradation curves for the P/N and N/P cells. The experimental points for the P/N cells were actually found to lie about midway between the predicted N/P and P/N curves and indicate that the lowest P/P_0 ratio observed was actually about 6% higher than the predicted P/P_0, i.e., the P/N cells were at least 6% higher in power than was predicted. Similarly, the N/P cells were from 3–6% higher in power than predicted. Since the damage coefficients for the P/N cell were derived from those of the N/P cell using Rosenzweig's factor of 6.2 (Ref. 6) between the coefficients at each proton energy, it is not too surprising that the P/N prediction was off by a higher percent than the N/P prediction. A factor of 4.0 (which is less conservative) is quoted in the *Handbook on Space Radiation Effects* (Ref. 4). Utilization of this factor would bring the P/N predictions more in line with the N/P predictions. However, this still leaves a 3–6% discrepancy between the predicted and the actual P/P_0 ratio. While the prediction technique was geared to be somewhat on the conservative side, as is indeed the case, one reason for the discrepancy might have been the dosimetry. If the dosimetry were such that the actual flux was smaller than indicated, the points would be shifted toward the predicted curve. In order to ascertain whether or not the results of these experiments are reasonable, the data were compared with results presented in published data. Since most of the

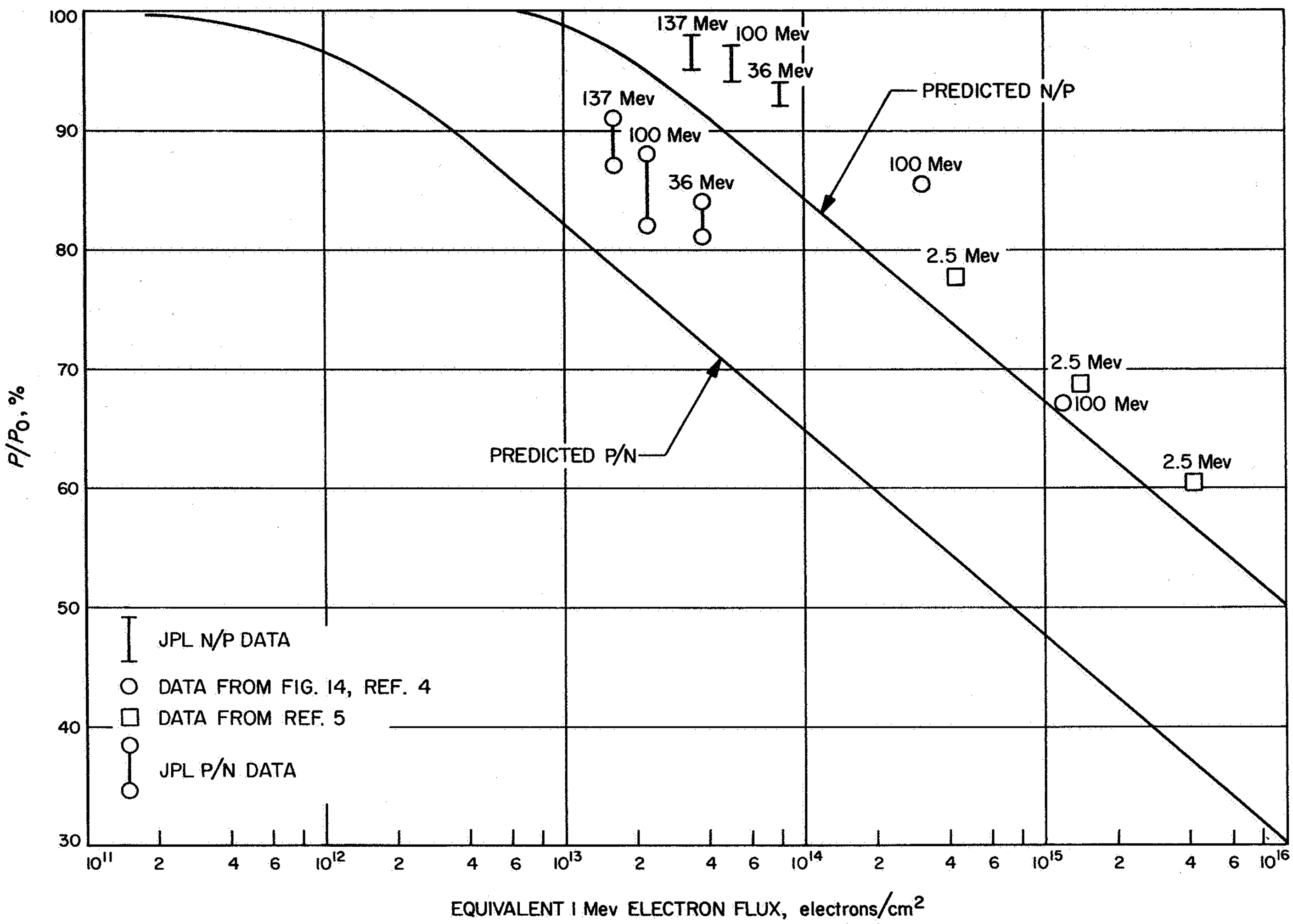

Fig. 6. Solar cell power degradation vs equivalent 1 Mev electron flux

existing proton data has been obtained on N/P cells (which was one of the compelling reasons for conducting these investigations on P/N cells) and since N/P cells have more consistent behavior with respect to radiation damage, some of the published data for this cell type have been plotted in Fig. 6, as indicated. The P/P_0 ratio was obtained from the published data and the reported flux was converted to equivalent 1 Mev electron flux. It can be seen that most of these points are greater than 3% higher in P/P_0 than the predicted curve. (Only one of the JPL points at 100 Mev is closer to the predicted curve than 3%.) In this respect, then, the data of this experiment seem to be in reasonable agreement with past experimental data. Another possible reason for the pessimism of the predicted P/P_0 is that the damage coefficients determined by Brown et al. (Ref. 7) may, themselves, be pessimistic since they were obtained for low excess carrier densities.

F. Conclusions and Recommendations

It is felt that this experiment has provided some extremely valuable information concerning the effects of high energy protons in silicon solar cells. It has been shown that there are no significant transient effects over the range of proton energies considered, even with flux densities as high as 10^7 protons/cm^2-sec. It has also been shown that the measurable electrical degradation is in the cell itself rather than in the coverslip adhesive for protons of these energy and flux density levels. For protons of these energy ranges, there was no discernable difference between shielded and unshielded cells. Individual cells exhibited degradations similar to modules fabricated from similar cells.

The predicted P/P_0 values were pessimistic by about 6–9% and 3–6% for P/N and N/P cells, respectively. While a discrepancy of this magnitude is not unreasonable considering the problems of correlating experiments performed by one laboratory to those performed by another with respect to flux dosimetry, cell electrical measurements, and variations of radiation characteristics from cell batch to cell batch, some possible explanations for these discrepancies have been given.

It is strongly felt that additional experiments of this nature would be helpful in making more accurate predictions of cell degradation due to exposure to solar proton flares. The dependence of the damage on the integrated flux dosage should be determined, since these experiments were done with only one flux level at each energy. Furthermore, the effects of protons of lower energies, from 4.5 Mev to 30 Mev, should be investigated since the great preponderance of damaging solar protons are within this energy range and there is very little experimental data of this nature on P/N cells.

VIII. CC&S Subassemblies

A. Test Setup

The following three subassemblies tested were mounted in a *Ranger* type half case as shown in Fig. 7a: (1) central clock, (2) end counter, and (3) maneuver duration. Testing consisted of subjecting the three subassemblies to proton irradiation of varying energy levels and flux densities, and in three mutually perpendicular planes as shown in Figs. 7a, 7b, and 7c. A test sequence was performed at each energy and flux density level, while being irradiated, to verify proper operation.

The irradiation was begun with the beam direction normal to the flat portion of the subassemblies. The energy was 137 Mev and flux densities varied in five steps from 1.46×10^6 protons/cm^2 sec to 1.94×10^7 protons/cm^2 sec.

The two other planes (normal to the bottom of the half case, and normal to the side of the half case) were then irradiated at maximum energy (137 Mev), and maximum flux density (about 2.0×10^7 protons/cm^2 sec).

The three planes were then individually irradiated at 99 Mev and 33 Mev, each at maximum flux density (about 2.0×10^7 protons/cm^2 sec.). The integrated fluxes which the units received in each orientation are shown in Table 11. Since only one subassembly of each type was available for this test, the total integrated flux for the assemblies is much higher than other test items received during the current program.

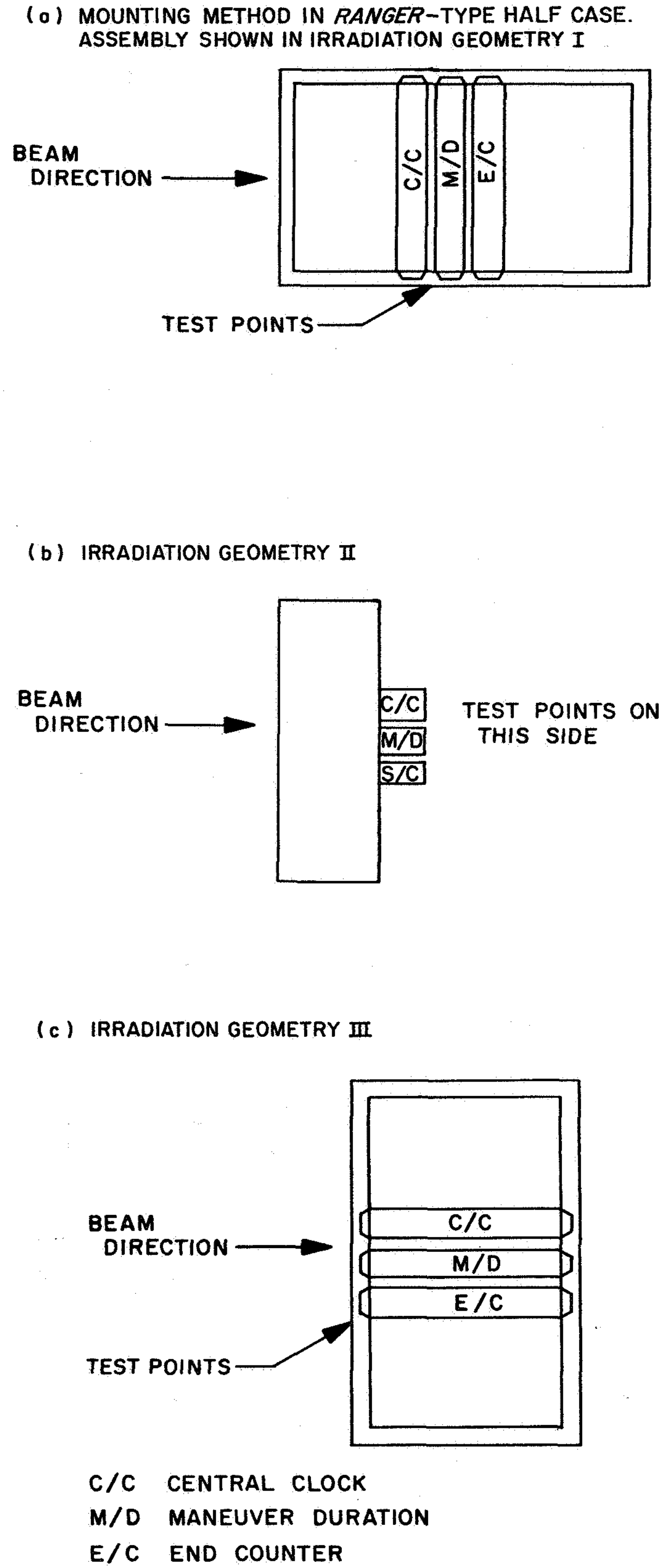

Fig. 7. Test setup for CC&S subassemblies

Table 11. CC&S subassembly test results

Run No.	Frequency,	E/C	Loading	M/D	Energy level, Mev	Beam time	Flux density, protons/cm^2 sec	Total flux, protons/cm^2	Int. flux, protons/cm^2
Beam normal to flat portion of subassemblies (Fig. 12a)									
Test	38.4003	ok	ok	ok	0	0	0	0	0
73	38.4003	ok	ok	ok	137	9.89	1.46×10^{6}	8.65×10^{8}	8.65×10^{8}
74	38.4003	ok	ok	ok	137	8.42	3.42×10^{6}	1.73×10^{9}	2.60×10^{9}
75	38.4003	ok	ok	ok	137	10.23	7.04×10^{6}	4.32×10^{9}	6.92×10^{9}
76	38.4003	ok	ok	ok	137	8.37	1.72×10^{7}	8.65×10^{9}	1.56×10^{10}
77	38.4003	ok	ok	ok	137	4.46	1.94×10^{7}	5.20×10^{9}	2.05×10^{10}
82	38.4003	ok	ok	ok	99	6.32	2.10×10^{7}	7.95×10^{9}	7.64×10^{10}
83	38.4003	ok	ok	ok	33	6.51	2.32×10^{7}	9.08×10^{9}	8.55×10^{10}
Beam normal to bottom of half case (Fig. 12b)									
78	38.4003	ok	ok	ok	137	12.23	2.00×10^{7}	1.47×10^{10}	3.55×10^{10}
81	38.4003	ok	ok	ok	99	6.45	2.01×10^{7}	7.78×10^{9}	6.84×10^{10}
84	38.4003	ok	ok	ok	33	6.44	2.24×10^{7}	8.65×10^{9}	9.42×10^{10}
Beam normal to side of half case (Fig. 12c)									
79	38.4003	ok	ok	ok	137	12.78	2.26×10^{7}	1.73×10^{10}	5.28×10^{10}
80	38.4003	ok	ok	ok	99	7.63	1.70×10^{7}	7.78×10^{10}	6.06×10^{10}
85	38.4003	ok	ok	ok	33	5.55	2.39×10^{7}	7.95×10^{9}	1.02×10^{11}

The test sequence included monitoring the 38.4 kc output of the central clock on a pulse counter, monitoring the times of relay closures in the end counter and verifying proper loading and shifting of the three maneuver duration shift registers. Maximum turns were loaded into each register and were timed with a stop watch in the speed-up mode. Nominal voltages were used during testing.

The steps of the test sequence are as follows:

1. Observe and record the count of the 38.4 kc central clock output.

2. Release the central clock inhibit, and time the relay closures of the end counter (using a stop watch and the speed-up mode).

3. Insert a single "one" into each maneuver duration shift register and verify that the register overflows. (This occurs if the previous overflow condition of all "ones" has not been altered.)

4. Insert a "zero" into each register and verify that it then takes 11 "ones" to cause an overflow. (This indicates that both "ones" and "zeros" can be inserted, and pre-loads each register for a maximum duration turn.)

5. Time the duration of the maneuver turns and motor burn, using a stop watch and the speed-up mode.

The data taken during the testing are shown in Table 11. The column headings indicate the following:

Run no.	Run no. recorded in the overall test log book
Freq	Counter reading of the 38.4 kc output (step 1)
E/C	Timing of end counter outputs (step 2)
Loading	Loading of maximum duration turns (steps 3 and 4)
M/D	Timing of midcourse turns and motor burn (step 5)
Energy level	Energy of the proton beam (units are Mev)
Beam Time	Time that the beam was on for that run (units are minutes)
Flux density (ave)	Average flux density for that run (units are protons/cm^2 sec)
Total Flux	Total flux for that run (units are protons/cm^2)
Int. Flux	Integrated flux up to that run (includes all previous runs in all planes. Units are protons/cm^2)

B. Test Results and Conclusions

No noticeable effects occurred during testing of the CC&S subassemblies. The 38.4 kc output was monitored to the nearest cycle and did not vary during any portion of the testing.

Proton irradiation to the energy and density levels tested does not cause any noticeable affect on CC&S operation. Testing did not verify temperature and voltage margins, however.

IX. Sun Sensor

A. Test Setup

The sun sensor consists of a pair of matched cadmium sulfide cells, the electrical resistance of which changes with the light intensity incident on the surface. In our application, two of the cells were connected in series to a center-tapped source of emf. Output of the device was then taken between this center tap and a connection between the cells. Knife edges, which are an integral part of the sensors, throw a sharp shadow on the center of each cell for a light source on-axis. When an equal amount of light falls on the cells, the output is zero; but if one cell receives more light than the other, the output will differ from zero, with a polarity which defines the cell with excess illumination.

For the proton testing, a jig was constructed which held two sun sensor assemblies, containing one CdS cell each, and a light source. This test fixture constrained the light source to remain on axis, resulting in a null output from the sensor. During the radiation testing this null output was monitored continuously with a recording voltmeter. The resistance of each cell was also measured periodically during the radiation.

Three sun sensors were irradiated during this test. Cells PTM APR1 7A11 and PTM APL1 7A13 were irradiated at 137 Mev; cells RA-3 APR2 7A11 and RA-3 APL2 7A13 were irradiated at 100 Mev; and cells RA-3 AYR2 7A10 and RA-3 AYL2 7A12 were irradiated at 33 Mev. In each case the exposure was 2×10^{10} protons/cm^2 at flux rates as high as 3.5×10^7 protons/cm^2 sec.

B. Test Results

No change in the parameters monitored was observed, either in a transitory or permanent manner, during the irradiations. The bombardments were usually carried out with the protons incident normally on the front cell surfaces. A test was also performed with the beam incident on one side of the fixture so that one cell partially masked the other. Here again no radiation effect was seen.

X. Canopus Tracker

A. Test Setup

The Canopus tracker was placed inside of a light tight wooden box with a 15×16 in. beam entrance window made of 2-mil aluminum foil. The tracker was held fixed with the left cover surface normal to the beam while a grain of wheat lamp, simulating Canopus, was driven back and forth in front of the tracker. A potentiometer pickoff of the angular position of the lamp drove the x axis of an $x\,y\,y'$ recorder. Brightness and roll error signals were monitored on the y and y' channels simultaneously.

Since the operational test showed that the tracker lost roll control during radiation at fairly low flux rates due to sensitivity of the optical system, some of the metal and glass components of a broken image dissector tube were isolated and irradiated separately. These pieces were then immediately placed in a counting system and checked for radioactivity. The system enabled a determination of half lives, energy spectra and type of particle to be counted.

B. Test Procedure

The irradiation procedure in this case differed from that used with the other subsystems because tracker performance was affected quite markedly by the proton beam. Therefore, flux failure thresholds at various incident proton energies were sought and an effort made to isolate the radiation sensitive components. To this end, 95 irradiations of the tracker were carried out in the energy range 19.5 to 137 Mev. Seventy-six irradiations were incident on the left cover surface for a total integrated flux of 2.1×10^{10} protons/cm^2, and 19 irradiations were incident on the front surface for an additional integrated flux of 2.8×10^9 protons/cm^2.

The tracker was assumed to lose its ability to track a star when the roll error signal dropped below 4 v peak to peak as the star simulator swept across the field of view. When the proton beam was incident on the tracker with no star in the field of view, the brightness voltage fell below its normal or beam-off value. It was observed that roll control loss occurred whenever the brightness voltage fell to 0.86 v (corresponding to a star brightness of about

8 × Canopus). Figures 8 and 9 are plots of the roll error and brightness voltages, respectively, as a function of 99 Mev proton flux. Here the roll control loss occurs at 5.6×10^5 protons/cm^2 sec. Similar curves were obtained at the other proton bombardment energies.

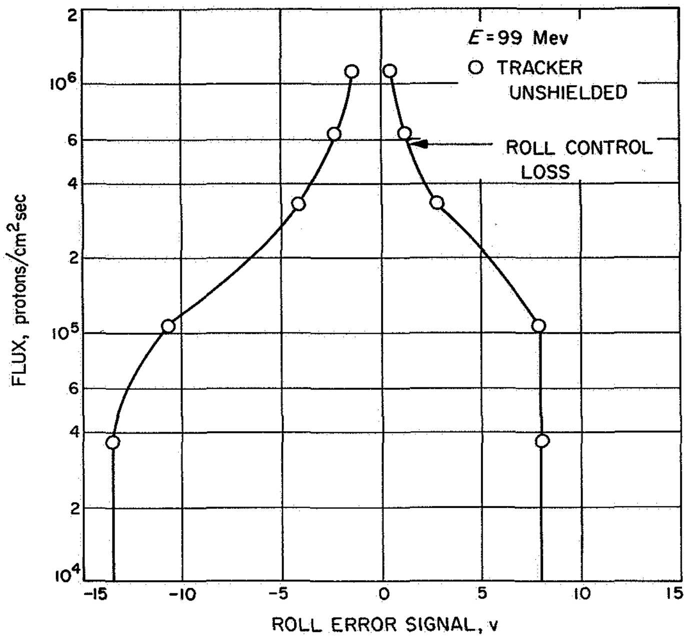

Fig. 8. Canopus tracker roll error signal as a function of 99 Mev proton flux rate

In order to isolate the areas of the tracker which were most susceptible to the proton radiation, various portions of the tracker were shielded from the beam. A plot of the resultant brightness voltage is given in Fig. 10 for a run at 137 Mev. A similar curve obtained at 33 Mev is given in Fig. 11. In Fig. 10 some dimensions are given associated with shield placements. These dimensions refer to distances measured from the front surface of the tracker. In this coordinate system, the lens extends from 3 to 4$\frac{5}{16}$ in., the fiber optics from 4$\frac{5}{16}$ to 4½ in., the deflection electrodes from 5¾ to 7¼ in., and the dynode region from 7⅝ to 10 in. It can be seen from Fig. 10 that the systematic marching of a 2-in. vertical shield across the tracker was never effective in blocking the beam from the radiation sensitive area, presumably because the sensitive area was wider than the 2-in. strip. Blocking the entire optical axis with a 2-in. shield does, however, reduce the radiation sensitivity considerably, but the effectiveness of the axis shielding is reduced considerably by moving the shield back far enough to expose the front lens element. In the 33 Mev bombardment, the same shielding experiment was

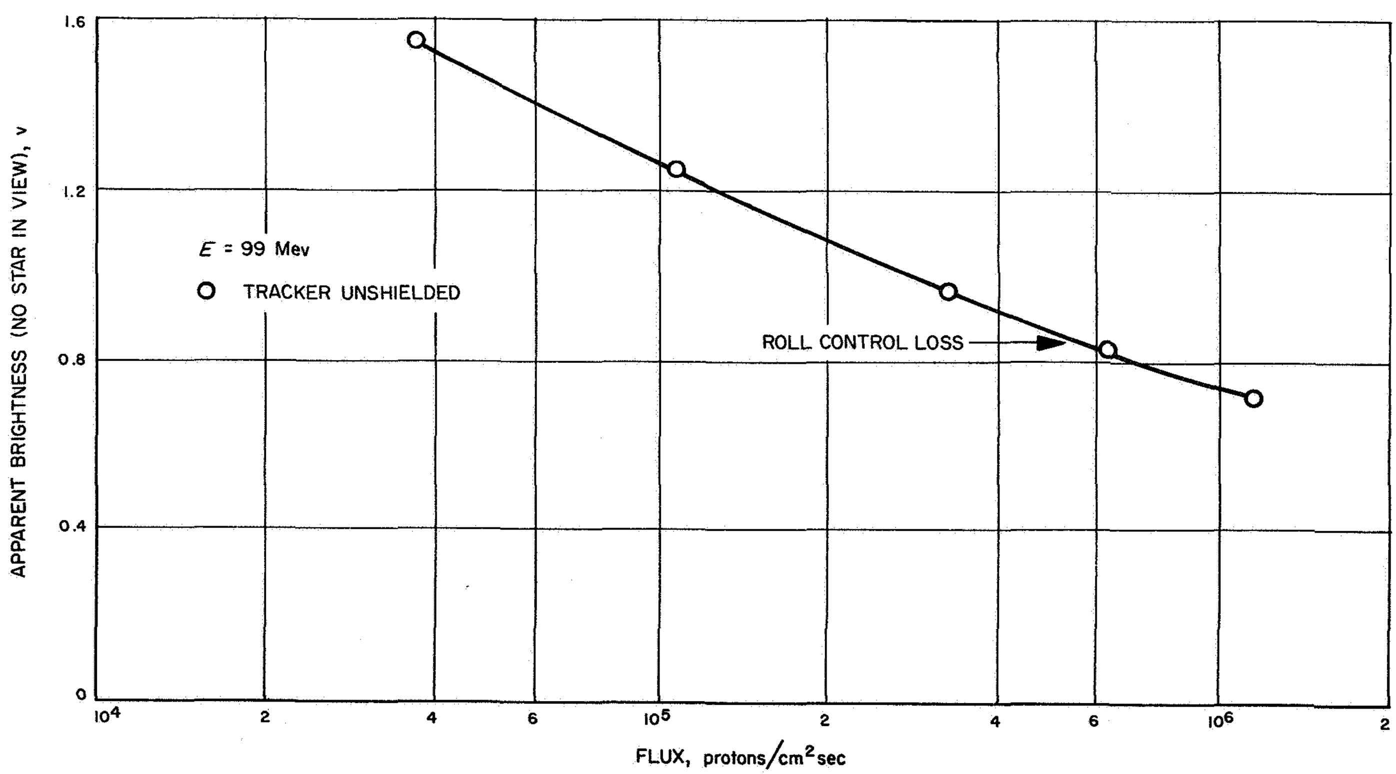

Fig. 9. Canopus tracker brightness voltage as a function of 99 Mev flux rate

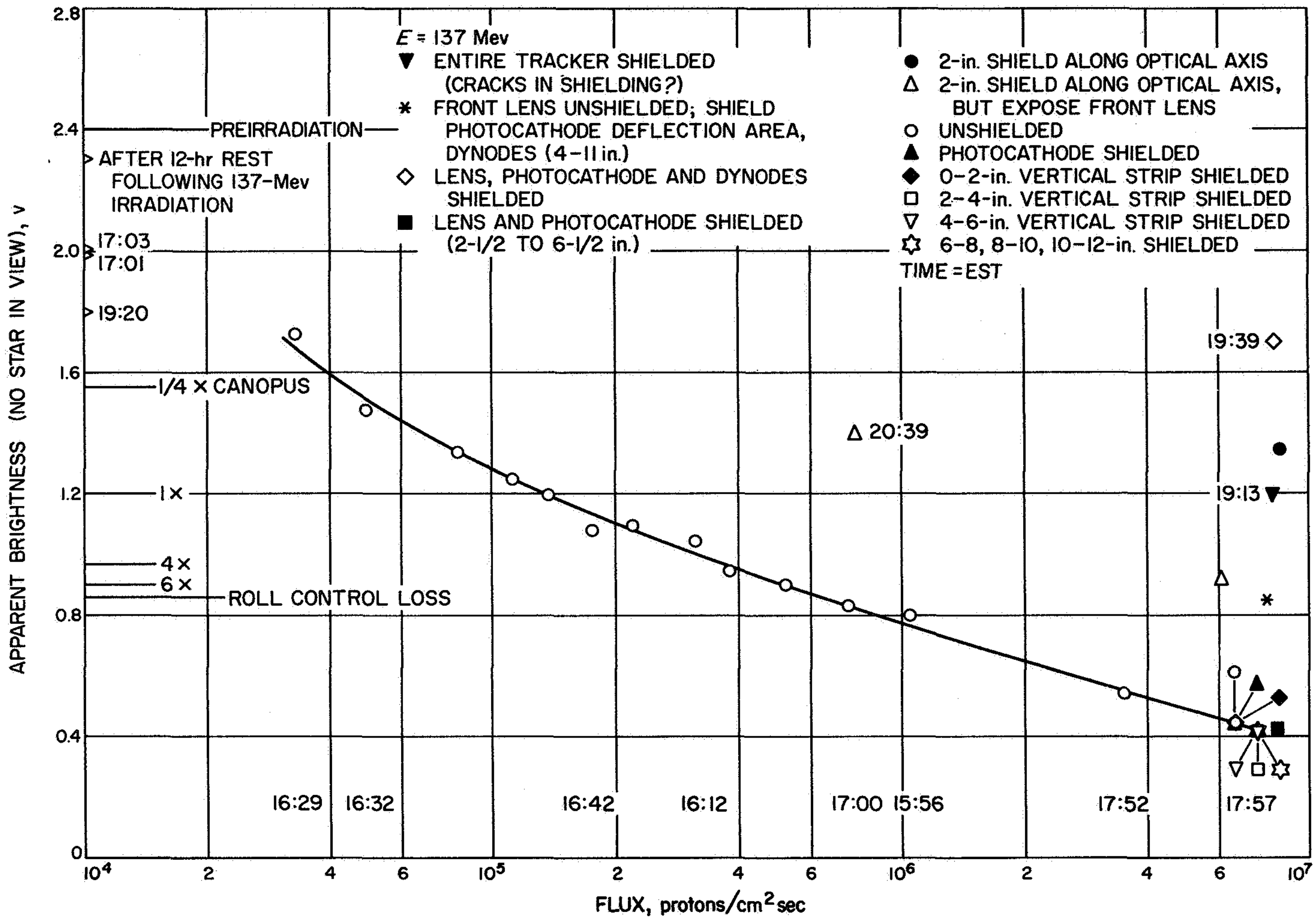

Fig. 10. Canopus tracker brightness voltage as a function of 137 Mev flux rate

performed, but here exposing the front lens element to the irradiation did not change the radiation sensitivity from that achieved with total axis shielding. High energy protons are therefore far more effective in degrading tracker performance than are low energy protons when incident on the edge of the front lens.

We note that when the dynode area is shielded from either the 33 or 137 Mev irradiations, the sensitivity of the tracker to proton radiation is substantially reduced. No shielding attempt changed the tracker response from the non-shielded curve unless the shield covered the dynode area. Figure 10 also shows the result of placing a shielding layer of lead bricks across the irradiated surface of the tracker. This shielding did not restore tracker operation to normal and leads one to conclude that some protons leaked into the tube through a crack in the lead brick wall. We conclude then that the entire dissector tube and particularly the dynode section appears to be sensitive to protons in the energy range used here.

Times (EST) of irradiation are given for several data points in Fig. 10. Beam-off brightness readings and times are also shown along the ordinate. The brightness reading at 1920 (after an approximate flux of $7 \times 10^{9*}$ protons/cm^2) is 0.6 v lower than the pre-irradiation value. After a total integrated flux of $9.6^* \times 10^9$ protons/cm^2 the tracker was allowed to rest for 12 hr during which the recovery was nearly complete. This semi-permanent behavior of the brightness voltage was presumed due to low level radioactivity induced by the proton beam in the image dissector tube, and led us to carry out subsequent proton activation experiments on portions of the tube.

*These integrated fluxes are values the tracker would have received if various shields had not been interposed during some of the irradiations, consequently they are somewhat high.

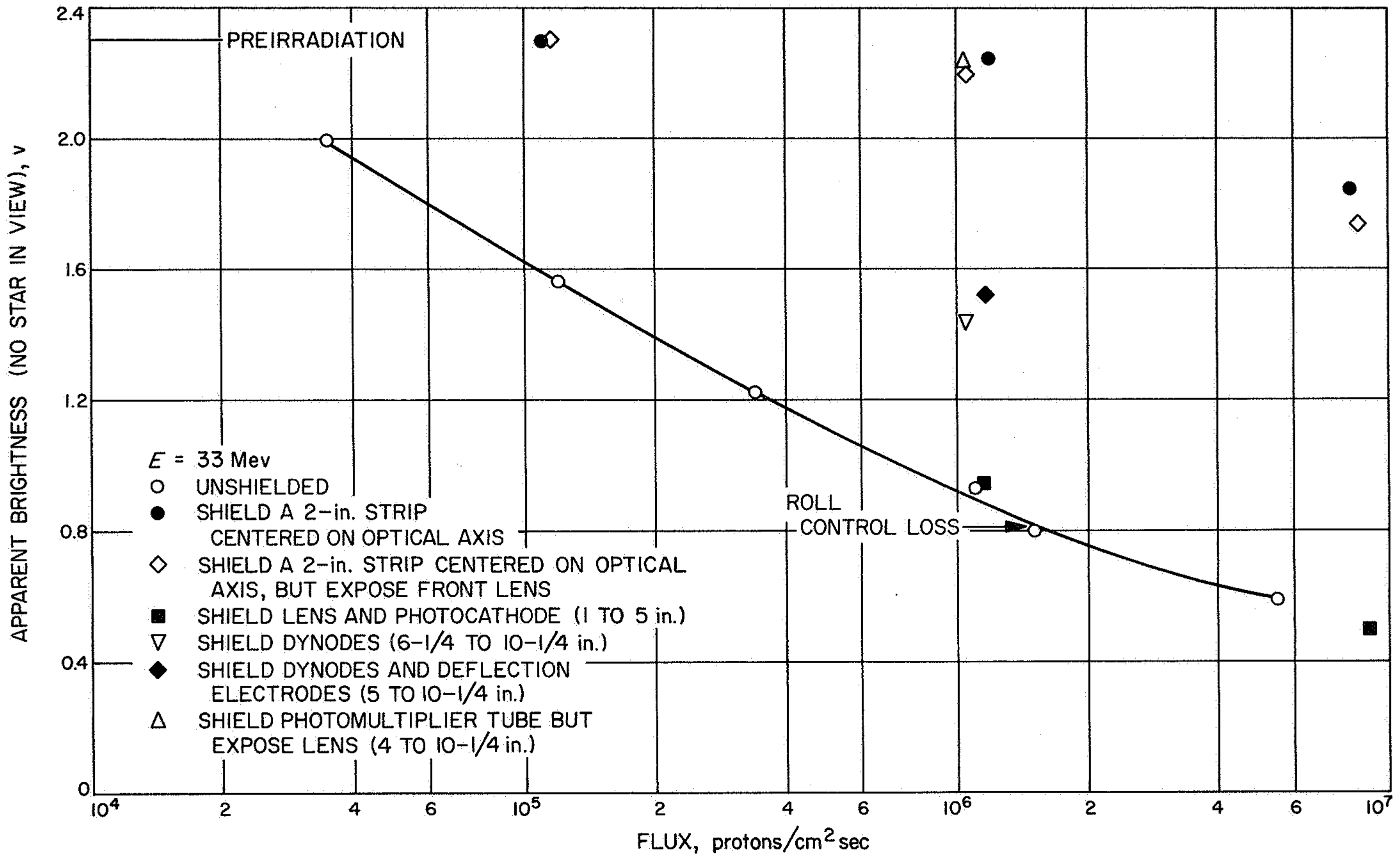

Fig. 11. Canopus tracker brightness voltage as a function of 33 Mev flux rate

Since our shielding experiments showed that the front lens element was radiation sensitive at higher energies, we bombarded the front surface of the tracker. Our irradiation fixture did not allow us room enough to sweep the artificial star across the tracker in this configuration, so we monitored only the brightness voltage, relating this to the previously observed failure points derived from the roll error curves. Figure 12 is a plot of the threshold fluxes required at each bombardment energy to cause roll control loss. Shown here are the failure threshold curves for both front face and side bombardments. Also shown are the required proton energies calculated to be necessary for penetration into the image dissector tube. This penetration energy falls roughly at the knee of each threshold curve, indicating that if the protons are energetic enough to penetrate the tube, a flux rate of 6×10^5 protons/cm^2 sec is adequate to cause tracker failure.

After exposing the image dissector tube to a proton flux of 10^{10} protons/cm^2, the exposed part was examined for radioactivity. The counting system consisted of a NaI(Tl) crystal, PM tube, Tennelec TC 170M preamp and a RIDL pulse height analyzer. The analyzer was used in the pulse height analysis mode to determine energy spectra and in the time sequence scalar mode to determine half lives.

It was not found possible to unambiguously identify the exact radioactive species activated by the proton beam. However, the metal dynodes as well as the glass did become quite radioactive, with the counter registering 2×10^4 counts/sec coming from the dynodes and 6×10^3 counts/sec from a glass portion (approx. volume 0.1 cm^3). These numbers are not corrected for counting geometry nor for the efficiency of our counter, hence the actual counting rates are probably at least two orders of magnitude higher. A ⅛ inch absorber placed between the test items and the detector did not appreciably alter energy spectra or counting rates, indicating that the activity was primarily gamma.

C. Test Results

In the time constant measurements for the decay of the activated dynode section, at least two decay rates were discernible. The short half life, 250 sec, compared favorably

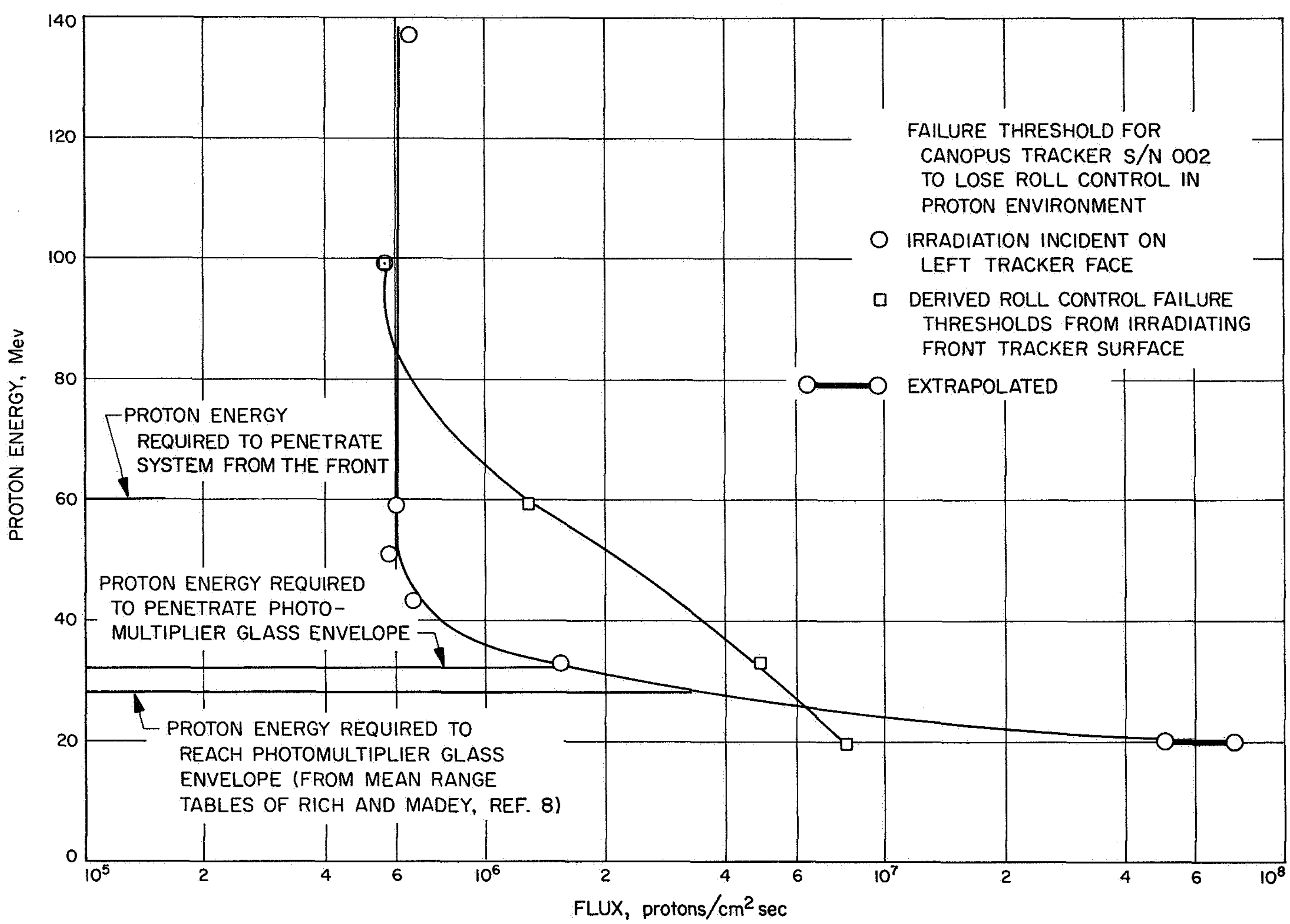

Fig. 12. *Failure threshold for Canopus tracker S/N 002 to lose roll control in proton environment*

with the previously observed initial half life for the brightness voltage recovery which was 290 sec. Following this fast initial decay there were much longer time constants observed for both the radioactive decay and for the brightness voltage recovery. However, the longer decay times were not accurately determinable from our measurements. The radioactivity induced in the glass alone was observed to decay with a half life of 180 sec.

Based on the results of these measurements, we can almost certainly conclude that the persistent but recoverable radiation damage induced by high energy protons in the tracker is due to radioactive activation of the image dissector tube.

It is interesting to note that the Canopus tracker failed at a flux of 6×10^5 protons/cm^2 sec for $E > 40$ Mev and at 2×10^9 electrons/cm^2 sec for 2 Mev electrons. The data encoder (Section IV), on the other hand, did not fail in proton fluxes as high as 10^7 protons/cm^2 sec, but failed at 10^9 electrons/cm^2 sec for 2 Mev electrons. That is, the data encoder is the more radiation sensitive subsystem of the two in an electron field, but the tracker is the more sensitive in a proton flux. For the tracker the ratio of the electron flux failure threshold to the proton flux failure threshold is 3.3×10^3, but the ratio of the proton stopping power to electron stopping power is only about 10. Therefore it is clear that the stopping power of the beam in the subsystem is not the main cause for the tracker failure in one or both of the radiation fields. It is therefore very dangerous to predict subsystem performance in a given type of radiation field even when the performance is known in another type of field. We think that the most likely explanation of this phenomenon here is a low radioactivity produced by the proton beam in the glass associated with image dissector envelope and optics as well as in the electron multiplier section.

Table 12. Microcircuits tested

Manufacturer	Part no.	Description	Case	Quantity
1. Fairchild	μL9040	Flip flop	Flat pack	6
2. Fairchild	μL9041	Gate	Flat pack	6
3. Fairchild	μA709	Operational amp.	Modified TO-5	1
4. Motorola	MC301F	Gate	Flat pack	3
5. Motorola	MC1526	Differential amp. (npn)	Modified TO-5	1
6. Motorola	MC1528	Differential amp. (pnp)	Modified TO-5	1
7. Texas Instruments	SN530	Flip flop	Flat pack	3
8. Westinghouse	WM201G	Gate	Flat pack	3
9. Westinghouse	WM202G	Flip flop	Flat pack	3
10. General Micro-electronics	R403	Flip flop	Modified TO-5	3
11. Norden	N1005	Differential amp.	Modified TO-5	2
12. Texas Instruments	SNX1503	Gate	Flat pack	3
13. General Micro-electronics	5232	Shift register	Flat pack	3
14. General Micro-electronics	5023	Shift register	Flat pack	1

XI. Semiconductor Devices

A. Description of Test Items

1. Microcircuits

Table 12 lists the microcircuits tested.

The items in Table 12 consisted of many transistors and components deposited on a single slab of silicon substrate. Items 13 and 14 also included deposited MOS transistors.

Item 12 and three each of items 1 and 2 were mounted on circuit boards and irradiated simultaneously with the data encoder (Section IV). These devices were not monitored during irradiation, but were checked for permanent damage afterward. They received the following irradiation: (1) 1.2×10^{10} protons/cm^2 at 30 Mev, (2) 1.2×10^{10} protons/cm^2 at 60 Mev, and (3) 1.1×10^{10} protons/cm^2 at 137 Mev. Each unit received radiation at only one energy. No bias was applied to any of these units tested during irradiation.

2. MOS transistors and photon switches

The following transistors were mounted on four circuit boards and irradiated simultaneously with the data encoder (Section IV): (1) Raytheon FN 1034, (2) GME 2N3608, (3) TI TIX511, (4) Fairchild FI100, (5) Motorola MM2102, (6) Motorola MM2103, (7) pnp bipolar transistor 2N995, (8) npn bipolar transistor 2N2369, (9) IBM developmental photon-coupled switch with GaAs diode, (10) TI developmental photon-coupled switch and GaAs diodes.

In addition to the above, six experimental light-coupled solid state switches manufactured by Texas Instruments and two GME 2N3608 MOS transistors were irradiated separately. The light-coupled switches consisted of a gallium arsenide diode and a photo-transistor assembled in an integrated circuit flat package in such a way that the infrared photons emitted by the diode, when it is forward biased, were incident upon the base region of the photo-transistor. The photons acted like base current in the photo-transistor, turning it on.

3. DAS Circuits: Logic circuits, discrete circuits, and bipolar analog to pulse width converters

Representative portions of MV-67 DAS were subjected to proton radiation, and the operation of the circuits tested was observed at energy levels of 33, 99 and 137 Mev. The flux levels varied from about 1×10^4 to 2.95×10^7 protons/cm^2 sec.

Test Items

The logic circuits tested consisted of four counters on the DAS test laminate:

1. Six bits of the 20-bit trapped radiation detection (TRD) counter
2. The bit counter
3. The word counter
4. The 444 kHz to 55.5 kHz countdown

These circuits consisted of the following Signetics integrated circuit types and quantities: two SE 424J, one SE 480J, two SE 416J, five SE 455J, one SE 156J, and one SE 731J.

Seven DAS discrete circuits were investigated: (1) crystal oscillator (with a 437.9 kc crystal), (2) 8-v pulse driver, (3) planet sensor line receiver, (4) analog to pulse width (A/PW) output receiver, (5) power on reset, (6) power supply monitor, and (7) isolated signal (IS) switch No. 1. The discrete circuits consisted of the following active parts plus numerous resistors and capacitors: eight 2N1711, six 2N914, four 2N995, seven FD 643, four zener diodes, one crystal, four transformers, PE 6161, one SE 180J, two SE 156J, and one SE 455J. These circuits were assembled on plug-in circuit cards.

A bipolar A/PW converter was also tested. The active parts consisted of: eight FD643, one FD306, two IN754, four FA3410U, two 2N708, two 2N901, five 2N930, one 2N2642, and four L2597's.

B. Test Setup

1. Microcircuits

A target of 11 test sockets was wired to accommodate one part of each of the first eleven part types listed in Table 12. The sockets were arranged in a planar array of approximately 4×5 in. and placed very near the beam center with the y axis directed at the source.

Following is a brief summary of the test procedure:

1. Read and record initial measurements for each of the components.
2. Perform steps 3–6 with proton energies of 137, 99, and 33 Mev, in that order.
3. Irradiate the components and read and record measurements while the beam is on.
4. If any change is detected during "beam on" measurements, take a set of "beam off" measurements.
5. Through a series of repeating steps 3 and 4, accumulate a total integrated flux of approximately 2×10^{10} protons/cm^2.
6. At the conclusion of the run, read and record measurements. For those part types with quantities of 2 or more, change units for the next energy run.

Additional testing:

7. Irradiate the unit with 137 Mev protons to accumulate a total integrated flux of 10^{12} protons/cm^2 with periodic reading and recording of measurements.
8. Read and record final measurements.

The amplifiers were wired for a gain of 20 and operated in a dc mode. The amplifier input levels remained constant throughout the test and the output voltage was monitored with a digital voltmeter.

All supply voltages to the gate circuits were held constant during testing. Dual gate samples were connected in series. A pulse generator operating at 60 Hz was connected to the gate inputs. The pulse amplitude was then lowered to the point where the gate under test failed to operate. Pulse amplitudes were monitored with a digital voltmeter to an accuracy of 1 part in 10^4.

The flip flops were connected so that they would trigger on a clock pulse from the pulse generator. Again the pulse amplitude was lowered to the point where the flip flop under test became inoperative and the resultant pulse amplitude recorded.

The shift registers (Items 13 and 14 in Table 12) were connected in series so that a binary signal (1, 0) applied to the input of the first would propagate through all. The output waveform of the 4th shift register was monitored on an oscilloscope so that failure of any of the registers would be observed. The range of shift register power supply voltage, for normal operation, was the parameter measured. The 4 units were mounted within the 95% isoflux contour of the beam with their flat tops facing the beam. These units were irradiated simultaneously with the above devices and to the same integrated flux at each energy.

2. MOS transistors and photon switches

The items irradiated with the data encoder received: (1) 1.2×10^{10} protons/cm^2 at 30 Mev, (2) 1.2×10^{10} protons/cm^2 at 60 Mev, and (3) 1.1×10^{10} protons/cm^2 at 137 Mev. They were not monitored during irradiation, but were checked for permanent damage afterwards.

Two of the GME 2N3608 MOS transistors were monitored during irradiation with the instrumentation shown in Fig. 13. The parameter measured was gate threshold voltage V_T at a constant drain current. Gate threshold voltage is the gate voltage necessary to cause a drain current of 100 μ amp to flow (with $V_D = V_G$) with the body and source connections grounded. The drain current was held constant by adjustment of the power supply voltage.

These MOS transistors were each irradiated to 2×10^{10} protons/cm^2 at 137, 99, and 33 Mev. An additional intense 137 Mev irradiation was administered at a flux rate of 1.4×10^8 protons/cm^2 sec, giving each unit an integrated flux of 8×10^{11} protons/cm^2.

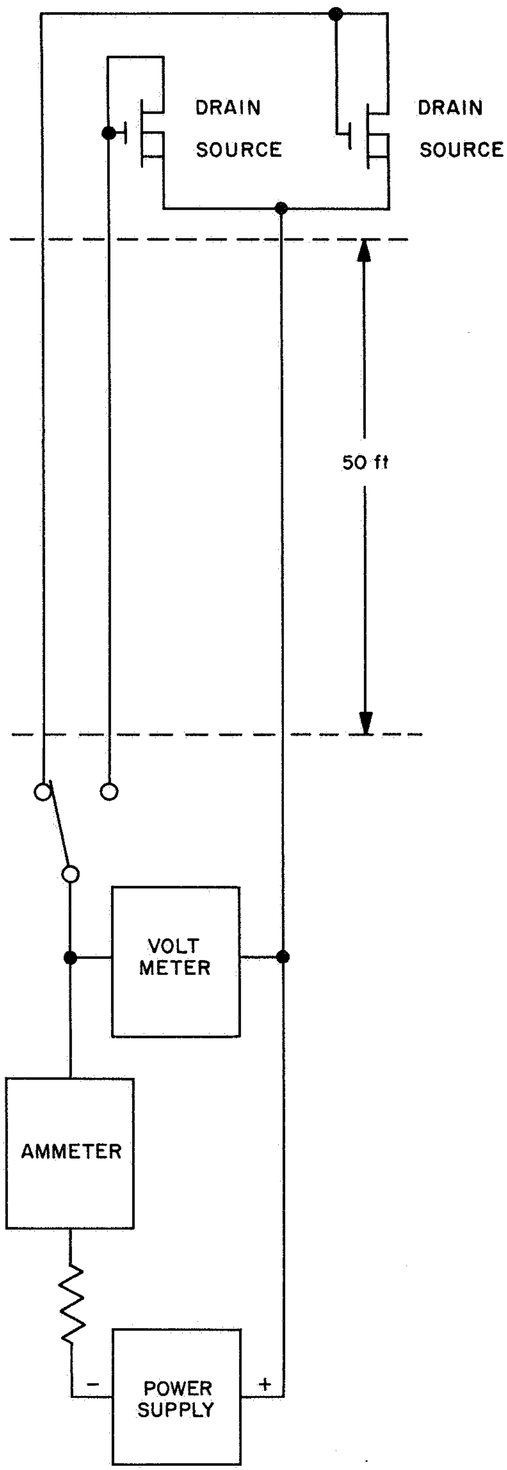

Fig. 13. Test setup for MOS transistors

Six of the experimental Texas Instruments photon switches were monitored during irradiation. The parameters of interest were: (1) transient irradiation effects on the leakage current of the photo-transistor (I_{CEO}), and (2) permanent effect on the photon emission characteristics of the diode, and on the gain of the photo-transistor.

The diode-transistor pairs were mounted in the center of the beam at the test plane with the flat surface of the packages perpendicular to the beam. Unit No. 1, designated the control unit, was shielded from the beam with a lead brick. It was used to indicate the amount of stray electrical pickup. The other 5 units received full beam strength. Leakage current was monitored as shown in Fig. 14.

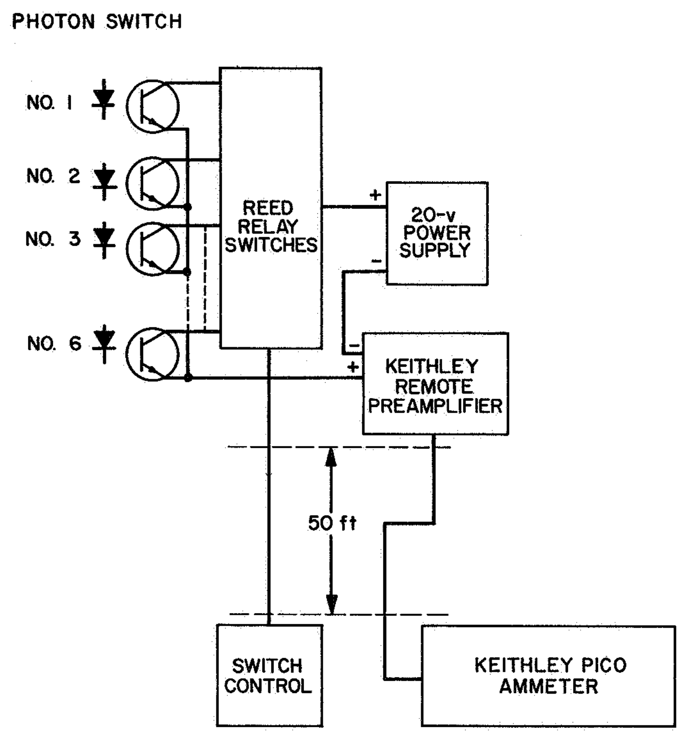

Fig. 14. Test setup for measuring leakage current in photon switches

3. *DAS Circuits*

The test setups used are shown in Figs. 15 through 17. All the circuits except the crystal oscillator, power supply monitor and A/PW converter were monitored for voltage margin during irradiation. The crystal oscillator was checked for frequency stability, and the A/PW converter was checked for deviation from previously determined linearity. The power supply monitor circuit was checked for the points at which the high and low voltage indications occurred.

Failure (margin level) of the logic circuits was defined as the point at which the count was no longer correct.

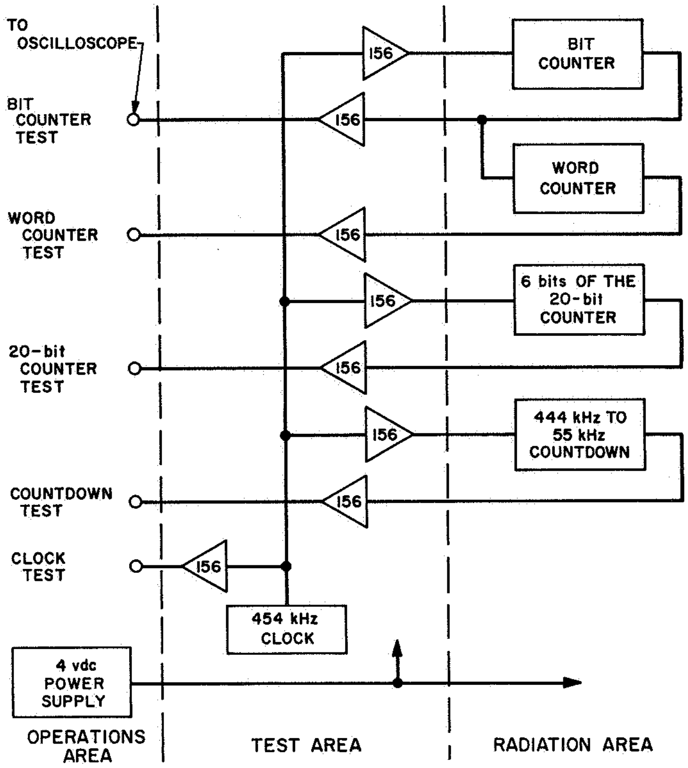

Fig. 15. Logic test setup for DAS counters

These circuits were also monitored for false counts at voltage levels near the margin level during irradiation. Some false counting was observed but was traced to noise from a large electro-mechanical counter on the accelerator control console.

The discrete circuits were monitored for the following failure conditions. The 8-v pulse drive output was monitored for the supply voltage at which the output pulse amplitude dropped to 3 v. Planet sensor line receiver was monitored for the supply voltage at which it no longer responded to simulated planet sensor output levels. The A/PW output receiver was monitored for the point at which it no longer responded to a 4 v input pulse. The power-on-reset was checked for the point at which it no longer switched. The IS switch no. 1 was monitored for the point at which the output transistor turned off.

C. Test Results

1. Microcircuits

The gates, flip flops and amplifiers showed only minor variations in the parameters measured. The cause of the variations could not be conclusively assigned to the radiation. The parameters measured during the test were fairly gross, however, and would not show fine parametric degradation. The amplifiers in particular would have to have been degraded drastically before any indication would show up in these measurements. It does appear that these integrated circuits will survive at least a 1-yr exposure to solar flare irradiation with no protective covering. It is recommended that future tests should be instrumented for the fine measurement of leakage current and/or gain in these circuits.

Variation of the minimum power supply voltage to operate the MOS shift registers is shown in Fig. 18. Also shown are the proton test energies used. Since we had a limited number of samples, the same units were exposed to an integrated flux of approx. 2×10^{10} protons/cm^2 at each test energy, then given an extra exposure at a rate of approx. 1.4×10^{8} protons/cm^2 sec to an integrated flux of 8×10^{11} protons/cm^2 using 137 Mev. As Fig. 18 shows, the greater sensitivity of the MOS register to 33 Mev protons caused a discontinuity in the minimum operating voltage. This discontinuity is not as apparent in the V_T curves of the 2N3608 MOS transistors irradiated concurrently (Fig. 19).

On the basis of these tests we conclude that the microcircuits will operate satisfactorily for at least a yr in space during a solar cycle maximum. Further testing at lower energies may be valuable, however.

2. MOS transistors and photon switches

The items irradiated with the data encoder and checked later for permanent parameter changes were found to exhibit the following behavior: (1) 40% increase in "on" resistance, (2) 10% decrease in transconductance, (3) 10% increase in average leakage current, and (4) no change in breakdown or threshold voltages. There was a 3% decrease in bipolar transistor beta and a 10% increase in photon switch "on" resistance. No energy dependent effects could be determined.

Transistor threshold voltage (V_T) change of the 2N3608 MOS transistor during irradiation is shown in Fig. 19. The different energies used are also shown. The results are as expected and these transistors should be capable of reliable operation for at least one year during solar maximum.

The results obtained in measuring the increase in I_{CEO} of the photo transistors are given in Table 13 for beam energies of 137 Mev.

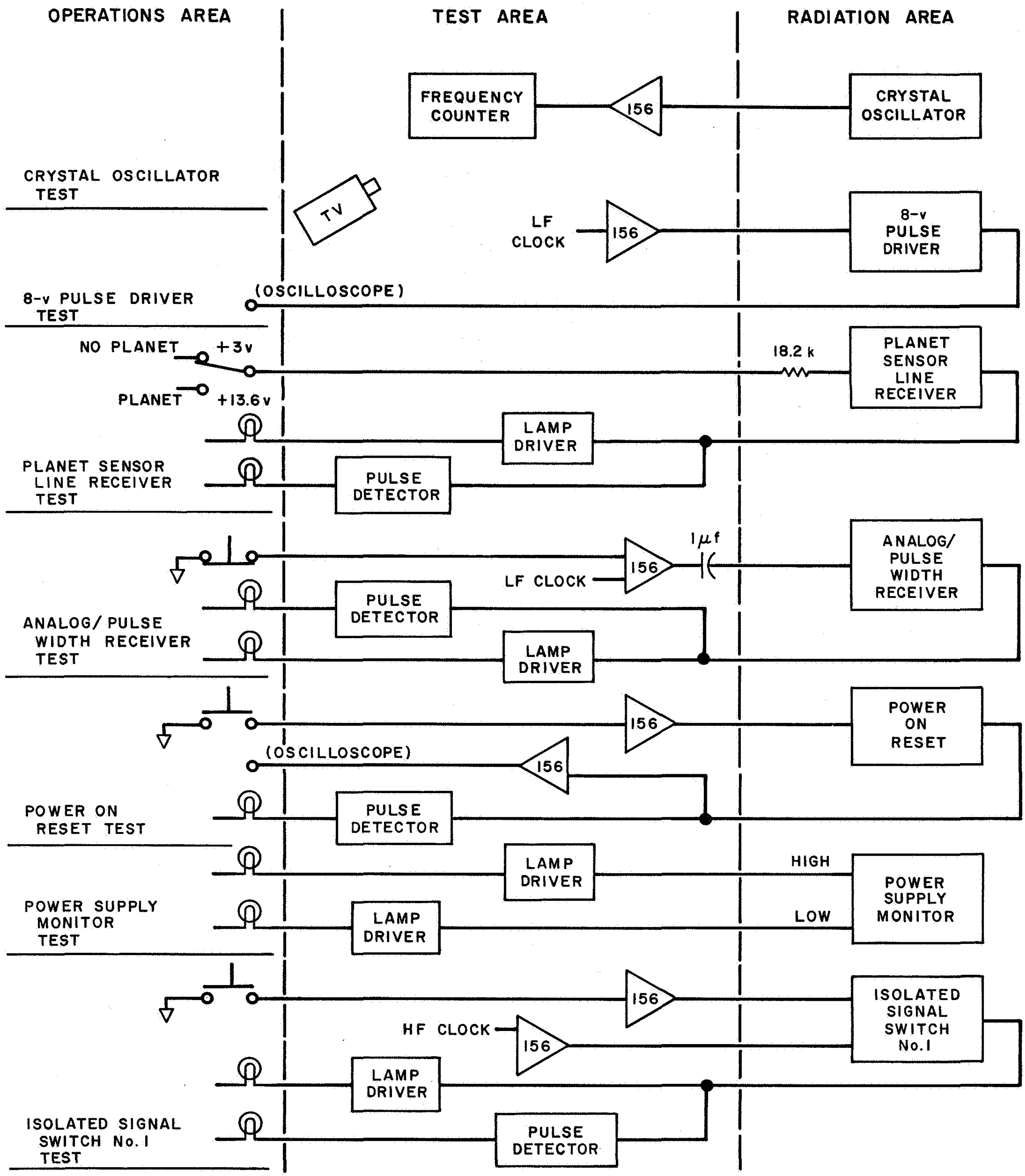

Fig. 16. DAS discrete circuit setup

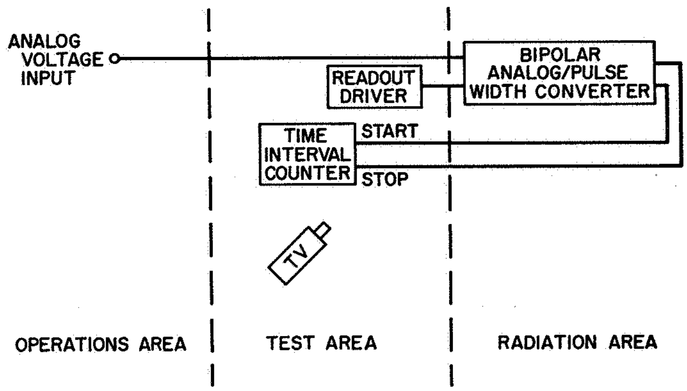

Fig. 17. DAS AP/W converter test setup

Other beam energies were tried at the flux rate of 2×10^7 protons/cm² sec. The energy dependence of I_{CEO} is shown in Fig. 20. The total integrated dose in this test was 2×10^{10} protons/cm², which is assumed to be equivalent to 1 year in outer space during a period of maximum activity. Table 14 gives leakage currents before and after irradiation. The changes are small and may be due to instrumentation drift.

Table 13. I_{CEO} increase of photo-transistors under proton irradiation

Unit	I_{CEO}, na			
	Proton flux rate, protons/cm² sec			
	4×10^5	1×10^6	2×10^6	2×10^7
1	—	0.5	—	2
2	1	—	2.5	17
4	—	—	1	7
5	—	1.5	—	9
6	—	2	—	15
7	1	—	—	16

Table 14. I_{CEO} of photo-transistors before and after irradiation

Unit	I_{CEO}, na	
	Before	After 2×10^{10} protons/cm²
1	5	4
2	5	4
4	8	7
5	24	25
6	18	16
7	28	30

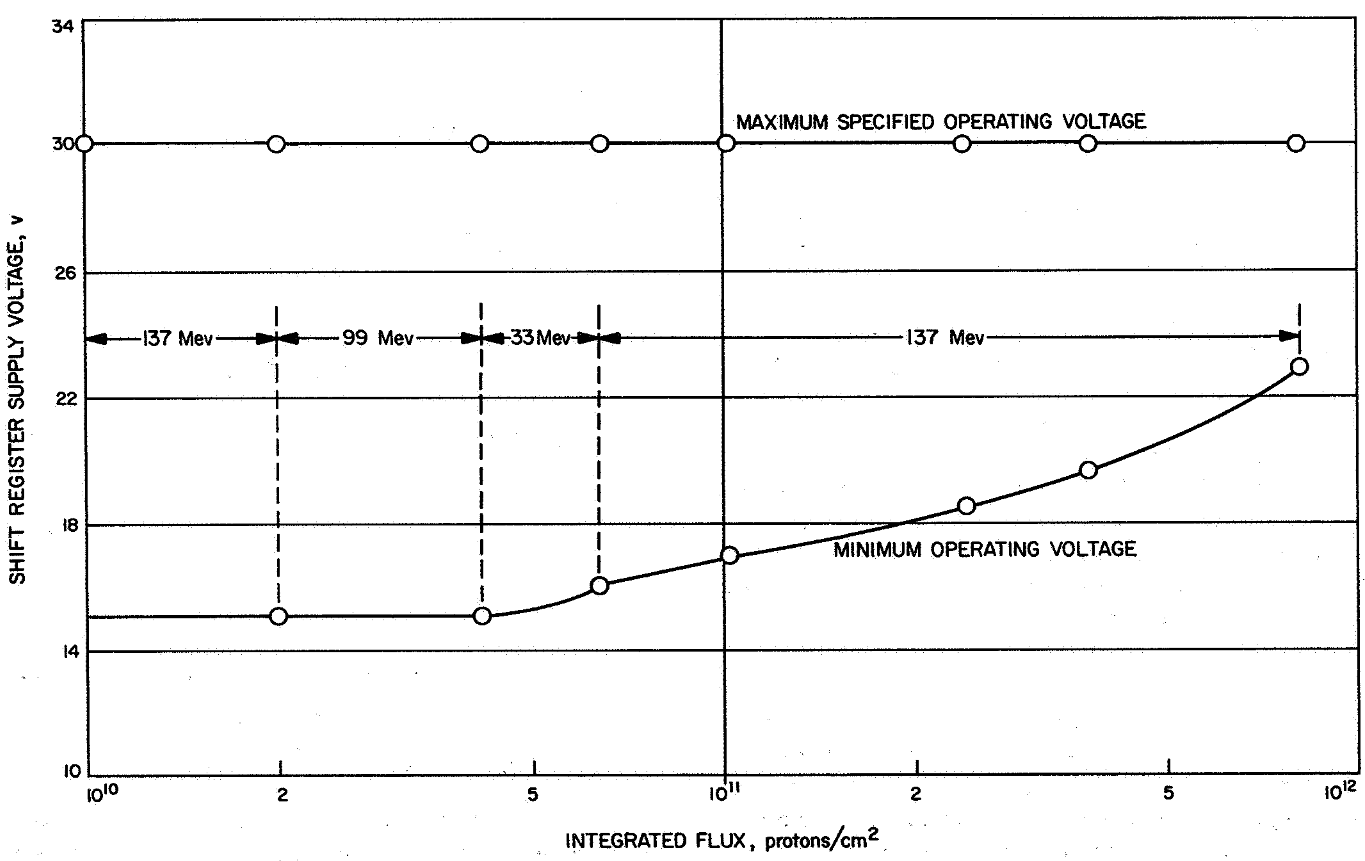

Fig. 18. Shift register supply voltage range vs integrated proton flux

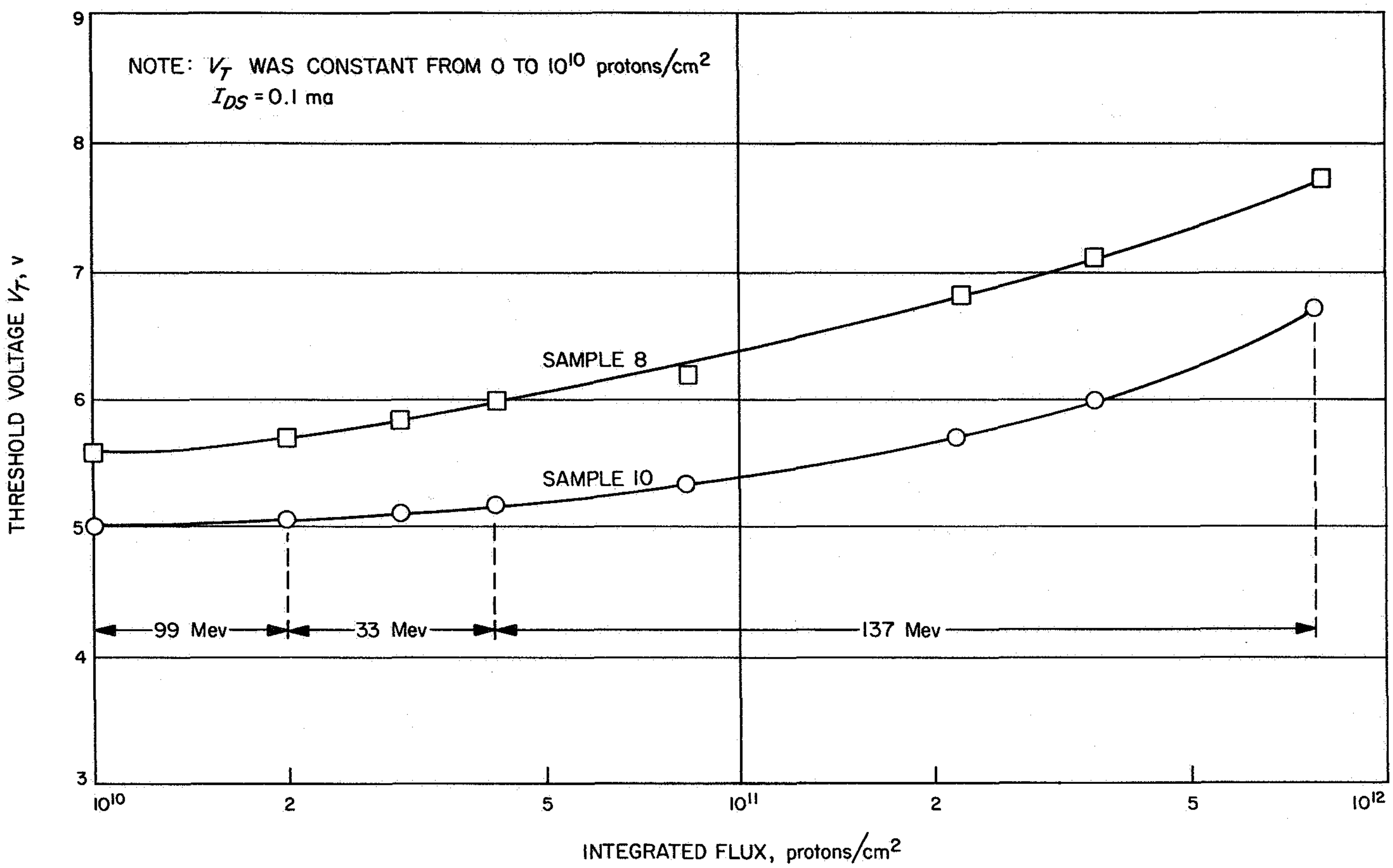

Fig. 19. V_T vs integrated proton flux for 2N3608 MOS transistors

The GaAs diode light emission efficiency and phototransistor gain were unaffected by the irradiation.

In summary, the results of this test indicate that the light-coupled, solid state switches, now under development for JPL by Texas Instruments, Inc., are not adversely affected by the flux rates or integrated doses of proton irradiation used. In the years 1956–61, a period of maximum solar activity, the largest event observed was estimated to be 5×10^4 protons/cm² sec. To get a nanoamp transient increase in leakage current we had to exceed that flux rate by a factor of $8 (4 \times 10^5)$. The transient increases observed at the flux rate of 2×10^7 would not be objectionable in most applications.

The energy dependence of transient leakage current is explained as follows. As the energy of particles entering the transistor is reduced, the proton energy loss per unit path length (stopping power) increases, forming more ion pairs, which in turn cause an increase in the leakage current. Since the curves of Fig. 20 must reach a maxima

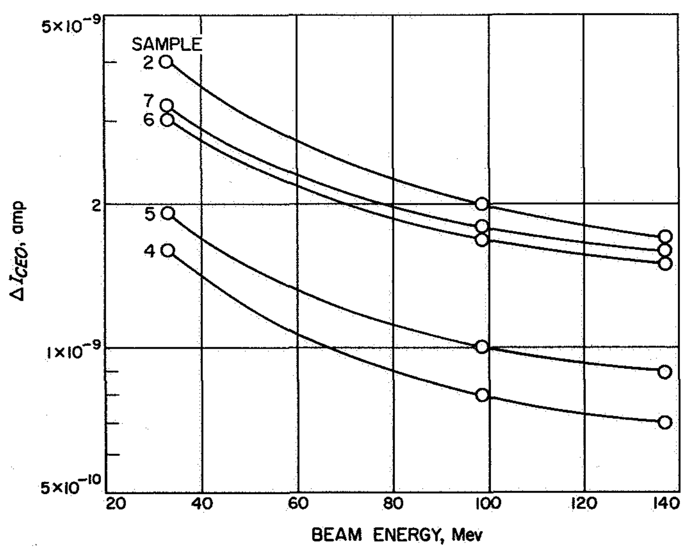

Fig. 20. Beam energy vs ΔI_{CEO} of photo transistors

at some lower energy, it may be advisable to carry these measurements out in lower energy regions, since most solar flare protons have E < 30Mev.

3. *DAS Circuits*

No failures or abnormal circuit operations were noted during or after the proton irradiation. The voltage margin point for the logic circuits was within 0.070 v (<2% variation) of the pre-radiation level. This small variation can be attributed to the subjectiveness of failure point determination. The same is true for the small variations noted on the discrete circuits at the A/PW converter.

Based upon our tests, the DAS should experience no failures, either temporary or permanent, caused by proton radiation in the energy ranges and flux levels run during these tests.

References

1. McDonald, F. B., Editor, *Solar Proton Manual,* NASA, TR R-169. National Aeronautics and Space Administration, Washington, Dec. 1963.
2. *Supporting Research and Advanced Development,* Space Programs Summary 37-34, Vol. II, p. 2. Jet Propulsion Laboratory, Pasadena, Calif., July 31, 1965.
3. Nicholson, M. M., Recht, H. L., and Kelchner, R. E., *Effects of High-Energy Protons on Selected Cells,* Final Report No. AI-66-149, Atomics International, Canoga Park, Calif., 1966.
4. Cooley, W., Janda, R., and Shivanandan, K., *Handbook on Space Radiation Effects to Solar Cell Power Systems,* NASA Contract NASW 598. National Aeronautics and Space Administration, Washington, July 22, 1963.
5. Reynard, D. L., *Proton and Electron Irradiations of N/P Si Cells,* LMSC 3-56-4. Lockheed Missile and Space Corp., Sunnyvale, Calif., April 12, 1965.
6. Rosenzweig, W., Smits, R. M., and Brown, W. L., "Energy Dependence of Proton Irradiation Damage in Silicon," *J. Appl. Phys.,* Vol. 35, No. 9, Sept. 1964.
7. Brown, W. L., Gabbe, J. D., and Rosenzweig, W., "Results of Telstar Radiation Experiments," *Bell System Technical Journal,* Vol. 42, No. 4, July 1963.
8. *Range–Energy Tables,* Laboratory Report No. 2301, University of California Radiation Laboratory, Berkeley, Calif., 1954.